Meteotsunamis in the northern Baltic Sea and their relation to synoptic patterns

Havu Pellikka [a,b], Jadranka Šepić [c,*], Ilari Lehtonen [b], Ivica Vilibić [d]

[a] *Department of Built Environment, Aalto University, Espoo, Finland*
[b] *Finnish Meteorological Institute, Helsinki, Finland*
[c] *Faculty of Science, University of Split, Split, Croatia*
[d] *Ruđer Bošković Institute, Division for Marine and Environmental Research, Zagreb, Croatia*

ABSTRACT

Low-tidal coastal regions, such as the Baltic Sea, are known to be particularly vulnerable to exceptional high-frequency sea level oscillations such as meteotsunamis. Possibilities of studying sub-hourly sea level variations have recently improved, owing to advancement in temporal resolution of tide gauge observations. In this work, we study high-frequency (period <6 h) sea level oscillations – strongest of which we consider to be meteotsunamis – on the coast of Finland, in the northern Baltic Sea, using quality-checked 1-min observations collected between 2004 and 2015 at 13 tide gauge stations. The intensity of the oscillations varies substantially between stations due to local coastal morphologies. The most intense oscillations predominantly occur in late summer and autumn, although the seasonality may differ between sub-regions. Measured atmospheric data and reanalysis products related to the strongest events reveal two distinct types of atmospheric processes and governing synoptic patterns that are mostly associated with warmer and colder period of year. Consequently, meteotsunamis are classified as summer-type or winter-type events. Most of the summer-type events are caused by surface atmospheric pressure jumps associated with mesoscale convective systems, which are advancing northward over the sea and are embedded into a mid-troposphere jet overtopping an inflow of warm low-troposphere air. At the surface, weak air pressure gradients due to a high-pressure area to the east and a low-pressure area to the west of the Baltic are usually found during summer-type events. The winter-type events, on the contrary, are mostly related to cold fronts and strong northerly-northwesterly-westerly winds at the surface layer. Contrary to summer-type events, surface atmospheric pressure jumps are not necessarily detected during the strongest winter-type events. Deep lows and extratropical cyclones are commonly centered to the north of the Baltic Sea and, at the mid-troposphere level, there is a pronounced westerly jet stream. A hypothesis about the generation mechanism of intense high-frequency sea level oscillations is given: Proudman resonance appears to be the main driver of summer-type events, whereas the main driver of winter-type events is less clear.

1. Introduction

Extreme sea level events in a changing climate pose a threat to coastal safety by causing hazardous situations in coastal traffic, damage to infrastructure, and loss of life (Taherkhani et al., 2020). The risk for damage increases if sea level changes are rapid and unexpected, occurring on time scales shorter than several hours, as this leaves little time for preparation. Sudden sea level changes also induce strong currents that may further increase the hazard.

Sea level oscillations at tsunami periods (from minutes to a few hours) may contribute significantly to sea level extremes, especially in low-tidal regions (Vilibić and Šepić, 2017). The tidal range in the semi-enclosed Baltic Sea is among the smallest in the world, with tides mostly reaching heights of only a few centimetres (Witting, 1911; Medvedev et al., 2013). Maximum storm surge heights are 1–1.5 m above the mean in central parts of the Baltic Sea and 2–4 m in its peripheries (Neva Bay, Gulf of Riga, Bothnian Bay, Kattegat, Belt Sea; Averkiev and Klevannyy, 2010; Wolski et al., 2014). Unexpected rapid sea level oscillations can lead to adverse impacts as the coastal infrastructure is not adapted to rapid and large variations of sea level. Better understanding of rapid variations and their formation mechanisms contributes to the possibility of forecasting such events and avoiding

potential damage.

Studies of sea level variations at tsunami timescales have, up till recently, been restricted by the time resolution of sea level measurements: typically, long records are available at a sampling rate of 1 h or longer. On the Finnish coast, in the northern Baltic Sea, continuous sea level measurements are available for most of the 20th century on the original paper charts of the pen-and-ink tide gauge recorders (Pellikka et al., 2020), but the digital database contains only hourly values up to 2003. Starting in 2004, the sampling rate of the Finnish tide gauge network has changed to 1-min. These measurements provide new insight into sea level variations occurring over shorter timescales.

Meteotsunamis (meteorological tsunamis) are one example of rapid sea level oscillations that are not captured by hourly measurements. Meteotsunamis are long ocean waves in the tsunami frequency band that are usually generated by air pressure disturbances moving over the sea at or close to a resonant speed (Monserrat et al., 2006). Meteotsunamis are further amplified by coastal topography and can reach destructive heights in extreme cases. Scientific studies of meteotsunamis in the Baltic Sea originate from the late 19th century. Unexpected high waves called Seebär have been discussed by Credner (1889), Doss (1906), Meissner (1924), Renqvist (1926), and Defant (1961). Renqvist (1926) conducted a case study of a Seebär event on the southern Finnish coast which occurred in May 1924. More recently, Pellikka et al. (2014) studied three 21st century meteotsunami events recorded by Finnish tide gauges. A systematic assessment of summertime meteotsunamis recorded by tide gauges in the Gulf of Finland between 1920s and 2014 (mostly extracted from pen-and-ink charts) has shown that most of the events (70%) are conjoined by pronounced short-lasting (tens of minutes) changes in air pressure, and that they occur during days with lightnings (Pellikka et al., 2020). The maximum height of the reliably documented events is ~1.5 m, with historical accounts pointing to even higher waves.

Along the world's coastlines, the strongest meteotsunamis are regularly associated with strong short-lasting air pressure disturbances which propagate over shelves with speeds of ~15–40 m s^{-1}, and which – through resonant processes (Proudman or Greenspan resonance; Proudman, 1929; Greenspan, 1956) – generate meteotsunamis (Monserrat et al., 2006; Rabinovich, 2020). In short, if the speed c of an atmospheric pressure disturbance is equal to the speed of the tsunami waves $\sqrt{gH}$, where g is gravity acceleration and H is the ocean depth, a strong amplification of the ocean wave is expected to occur through Proudman resonance (e.g., Vilibić, 2008). The same is valid for Greenspan resonance, but in this case, the speed of the atmospheric disturbance has to match the speed of the i-th mode of the edge wave. Also, travelling wind pulsations can generate meteotsunamis, being particularly relevant in shallow coastal regions (Šepić and Rabinovich, 2014).

Such atmospheric pressure disturbances and associated meteotsunamis frequently occur during specific synoptic conditions. Vilibić and Šepić (2017) found that the zonally-averaged range of high-frequency (T < 2 h) sea level oscillations is significantly (at 99%) and positively correlated with the wind speed in mid-troposphere. Strong mid-troposphere jets favour the generation of convective cells and internal gravity waves (Plougonven and Zhang, 2014) which can, at the surface, manifest as meteotsunamigenic air pressure jumps or waves. The mid-troposphere jet has further been associated with the high-frequency sea level oscillations in the Mediterranean, where it is frequently conjoined with a strong thermal front in the lower troposphere and a surface low detectable in mean sea level pressure (Šepić et al., 2015). These conditions are common for the strongest meteotsunamis in the Balearic Islands (Jansà and Ramis, 2021) and the Adriatic Sea (Vilibić and Šepić, 2009). The intense mid-troposphere jet has also been recognised as the key synoptic meteotsunamigenic variable in other regions, e.g., Australia (Vilibić and Šepić, 2017), Japan (Tanaka, 2010), the Great Lakes and the east U.S. coast (Šepić and Rabinovich, 2014), and the Persian Gulf (Heidarzadeh et al., 2020). However, such a

strong jet may appear during different atmospheric processes responsible for the generation of meteotsunamigenic atmospheric disturbances, in particular as the meteotsunami events are associated with different weather types around the globe (Rabinovich, 2020). Diversity in meteotsunami types exists, in particular, in upper mid-latitudes, like Northwest Europe (Williams et al., 2021).

In the northern latitudes, sea ice is another variable that should be considered when assessing conditions in which meteotsunamis and other nonseismic high-frequency sea level oscillations occur. Sea ice forms annually in the Baltic Sea and affects high-frequency sea level variations by preventing the effect of wind on sea surface and by attenuating or completely blocking wind waves. However, in contrast to wind waves, the ice cover does not completely suspend long period ocean waves or seiches, although it attenuates them (Sergienko, 2010; Marchenko and Morozov, 2016). The attenuation rate depends on the wave period and the properties of sea ice, mainly its concentration and thickness. The ice season on the Finnish coast varies greatly from year to year, from nearly ice-free conditions throughout the winter to a stable ice cover along the whole coastline (Schwegmann and Holfort, 2021). The ice season lasts from November to May in the northernmost parts of the Gulf of Bothnia.

In this study, we identify a number of high-frequency (T < 6 h) sea level events observed at the Finnish tide gauge stations between 2004 and 2015, then proceed to document and classify the atmospheric conditions that are conjoined with the events. Several research questions are put forward: (i) what is the geographical coverage and seasonality of the observed high-frequency sea level events, (ii) what kind of weather systems and synoptic conditions are conjoined with the events, and (iii) can these atmospheric processes be classified and ascribed to the known processes in other regions. Section 2 presents the sea level data and quality-control, the atmospheric data used and the selection process of the high-frequency sea level events. Section 3 provides statistics on the observed high-frequency sea level oscillations and documents the atmospheric properties conjoined with summer-type and winter-type events. Section 4 portrays the documented classes of weather systems and their seasonality, and discusses possible generation mechanisms responsible for both types of events.

2. Data and methods

2.1. Sea level data and quality control

The sea level data used in this study comprise 12 years (2004–2015) of raw 1-min observations from 13 tide gauges on the Finnish coast (Fig. 1). Sea level oscillations are compared with wind and air pressure observations from stations located near the tide gauges (Table 1). These weather observations originate from the database of the Finnish Meteorological Institute and have mostly a temporal resolution of 10 min.

To remove erroneous jumps and spikes from the sea level data, we performed a two-step quality control. First, we automatically despiked the data by removing data points that differ more than 15 cm from both neighbouring 1-min values, or by more than 20 cm from one of them. Such spikes can be considered erroneous, as we found – using spectral analysis (see also in Section 3.1) and checking the bathymetry data – that there are no processes at short periods, e.g. around 2 min, that might create lonely peaks in the series. Zero values also indicate errors in the system and were removed, as they are unrealistic in the height reference system used (the original bedrock-bound reference level of each tide gauge, about 2 m below the mean sea level in 1920). Second, a visual quality control was performed by plotting consecutive 15-day periods of the data and removing clearly artificial spikes, shifts and other obviously erroneous data. The amount of missing data before and after the quality control is presented in Table 1.

Not all problems in the data were solved by the quality control. Blocks in the pipe connecting the well of the tide gauge to the sea have resulted in significant damping of the sea level signal at some tide
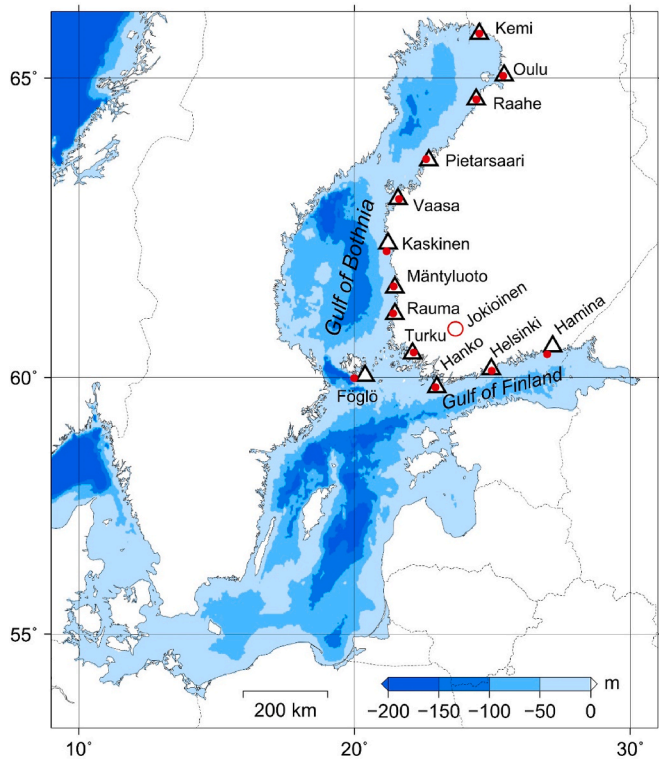
Fig. 1. Map of the Baltic Sea. The Finnish tide gauges and the closest weather stations, from which data was used in this study, are marked with triangles and red dots, respectively, and the radio-sounding station in Jokioinen with a circle.

Table 1
The percentage of missing 1-min observations (2004–2015) in raw data and after the quality control (QC) at the Finnish tide gauges. For the purposes of this study, the tide gauges are divided in two regions: the Gulf of Bothnia and the Gulf of Finland. Air pressure data is from nearby coastal stations; the last column gives the distance between the tide gauge and the weather station (km).

No.	Tide gauge	Region	Missing (%)		Weather station	Dist.
			Raw	QC		
1	Kemi	Gulf of Bothnia	3.0	3.0	Kemi, Ajos	0
2	Oulu	Gulf of Bothnia	5.2	5.7	Oulu, Vihreäsaari	4
3	Raahe	Gulf of Bothnia	3.2	4.6	Raahe, Lapaluoto	0
4	Pietarsaari	Gulf of Bothnia	26.9	27.7	Pietarsaari, Kallan	9.5
5	Vaasa	Gulf of Bothnia	3.9	4.5	Vaasa, Klemettilä	4
6	Kaskinen	Gulf of Bothnia	3.8	3.8	Kristiinankaupunki, Lighthouse	15.9
7	Mäntyluoto	Gulf of Bothnia	2.0	2.2	Pori, Tahkoluoto	6.1
8	Rauma	Gulf of Bothnia	2.0	2.0	Rauma, Kylmäpihlaja	6.7
9	Turku	Gulf of Bothnia	2.1	3.9	Turku, Artukainen	5.2
10	Föglö	Gulf of Bothnia	4.5	7.2	Lemland, Nyhamn	25.4
11	Hanko	Gulf of Finland	2.5	4.1	Hanko, Tulliniemi	3.9
12	Helsinki	Gulf of Finland	15.4	17.6	Helsinki, Harmaja	5.5
13	Hamina	Gulf of Finland	3.1	5.1	Kotka, Rankki	24.1

gauges (Raahe, Mäntyluoto, Turku) over certain periods lasting from weeks to months. There are also periods of discretized, stair-like data caused by bit errors at some stations (Oulu, Vaasa, Turku, Föglö), also lasting for weeks or months in some cases. Thus, not all rapid variations in sea level have been recorded correctly. These errors do not affect our main findings, because this paper focuses on a limited number of events recorded by multiple tide gauges.

After despiking the data, we removed the tides with the t-tide software (available for MATLAB, Pawlowicz et al., 2002). The amplitude of the tidal sea level variation is small in the Baltic Sea: diurnal components (K_1 and O_1) have amplitudes of 0.5–2 cm and semi-diurnal components (M_2 and S_2) have amplitudes of 0.5–1.5 cm (Leppäranta and Myrberg, 2009).

To identify rapid short-period sea level variations, we first applied a 6-h Kaiser–Bessel high-pass filter (shape parameter 3π) (e.g., Thomson and Emery, 2014) to the quality-controlled data. We then calculated the height of each individual wave from crest to trough (between two crests), where a crest was identified by a sign change in the derivative of the filtered sea level signal. This wave height dataset was then sorted in descending order. We chose the highest daily wave to avoid analysing the same event multiple times. This resulted in a dataset of uniquely dated high-frequency sea level events at each tide gauge.

2.2. Atmospheric data

A general overview of the weather situation during the meteotsunami events was based on an analysis of synoptic weather charts. In evaluating the speed of weather systems, we further used weather radar imagery, lightning detections, and station observations. In particular, air pressure as well as wind speed and direction were useful variables to examine in order to determine the passage times of weather fronts associated with the sea level events. The speed of weather systems was then evaluated by comparing observations from several adjacent stations. To detect lightnings, data from the Nordic Lightning Information System (Mäkelä et al., 2014) were used. The lightning data were the primary source for evaluating the propagation of mesoscale convective systems.

For the large-scale synoptic analysis of air pressure, wind and atmospheric stability, we used 6-h data from the European Centre for Medium-Range Weather Forecast (ECMWF) ERA-Interim reanalysis (Dee et al., 2011). We analyzed those variables which are known to have a distinct pattern during meteotsunamis in other parts of the world (Vilibić and Šepić, 2017): mean sea level pressure (MSLP), temperature at the 850 hPa level, and wind at the 500 hPa level. The atmospheric stability was estimated using the Richardson number (R_i):

$$R_i = \frac{N^2}{(du/dz)^2} \tag{1}$$

where N is the Brunt-Väisälä frequency, u is wind speed and z is height. We calculated the moist Brunt-Väisälä frequency (Durran and Klemp, 1982) on levels where the relative humidity was above 70%, and the dry frequency elsewhere (with the limit lifted to 90% for sounding data). The atmospheric layer is considered to be dynamically unstable if $R_i < 0.25$. Instability of atmospheric layers was examined for each studied event and classified as: "yes" – a wide area of dynamically unstable layers above the Baltic Sea, "some" – small scattered areas of dynamically unstable layers above or near the Baltic Sea, "no" – no dynamically unstable layers above the Baltic or in its vicinity.

Radio-sounding data measured at Jokioinen (Fig. 1) regularly, mostly every 12 h, were used to document the vertical structure of winds, temperature and dew temperature, as well as derived parameters: Richardson number, convective available potential energy (CAPE) and convective inhibition (CINS) that reflect the strength of convective processes or stability of the air column, as well as mean mixed-layer mixing ratio (MLMR) that quantifies the intensity of mixing in the

atmospheric boundary layer. Sounding data were collected from the University of Wyoming website at http://weather.uwyo.edu/upperair/sounding.html, for available observation times closest to the occurrence time of a meteotsunami event.

2.3. Selection and classification of meteotsunami events

Inspection of sea level series and synoptic conditions implies that meteotsunami events in Finland can be classified based on geography and season. Geographically, we divide all events into: (i) those occurring over the west-to-east oriented Gulf of Finland (3 stations: Hanko, Helsinki, and Hamina), and (ii) those occurring over the south-to-north oriented Gulf of Bothnia (10 stations, from Föglö to Kemi; Fig. 1, Table 1).

Seasonally, we classify events into:

 i) *summer-type events*, occurring in our analysis exclusively between late April and October, mostly associated to air pressure jumps measured at the surface, and – on a larger scale – to shallow weather systems with weak surface gradients of mean sea level pressure, i.e., relatively weak surface winds, and
 ii) *winter-type events*, occurring mostly between November and April (but with a few cases in May and June as well), mostly associated to cold front passages, and – on a larger scale – to deep extratropical cyclones overlying the area of the northern Baltic Sea.

It should be noted here that the months from November to April roughly correspond to the length of ice season on the Finnish coast, but ice conditions vary strongly from year to year. The Baltic Sea is ice-free during the summer season (May–Oct), although some ice usually remains in the northernmost parts of the Gulf of Bothnia until June. Nonetheless, all of our events have occurred during mostly ice-free conditions, just sporadically characterized with some coastal ice. The ice conditions were assessed qualitatively using daily ice charts covering the Baltic Sea.

From the dataset of maximum daily wave heights, for each station, we extracted all events during which the wave height surpassed the 97.5th percentile at that station, resulting in 7–9 events per station per year. We will refer to this dataset as the *Extreme wave heights dataset*. We did additional analysis on this dataset, which included spectral analysis, estimation of seasonal cycle, and estimation of the spatial distribution of extreme high-frequency oscillations wave heights. We further limited our dataset by selecting 5–10 of the strongest events during May–October and November–April seasons for each region for further analysis. The criteria for making the selection were (i) the number of tide gauges where significant high-frequency sea level oscillations were observed, and (ii) the maximum observed wave height.

Within the paper, we interchangeably use terms "(extreme/significant) high-frequency oscillations" and "meteotsunamis". There is an ongoing discussion within the scientific community on what constitutes a meteotsunami: (i) there are authors which suggest that only strongest events of atmospherically generated high-frequency (T < 2–6 h) sea level oscillations, i.e., only those events during which wave height surpasses a non-station specific threshold should be termed meteotsunamis (e.g., 100 cm for the Adriatic Sea meteotsunamis; Orlić, 2015; Šepić et al., 2022); (ii) there are authors which suggest that criteria for identifying meteotsunamis should be station specific (e.g., Rabinovich and Monserrat, 1996); and finally (iii) there are authors that combine both station and non-station specific criteria (e.g. Dusek et al., 2019). Following approach by Pellikka et al. (2020) for Finnish meteotsunamis, we chose to adhere to station specific criteria, and consider all events during which wave-height of 6-h filtered sea level oscillations was above 97.5 percentile value of maximum daily wave heights at a respective station to be meteotsunamis.

2.4. Proudman length

To evaluate whether bathymetry and orientation of the basins play a role in the formation of long open ocean waves through Proudman resonance, we quantified potential for Proudman resonance occurrence. Following the methodology by Šepić et al. (2016a), we choose a range of possible speeds (10–50 m s^{-1}, with a step of 1 m s^{-1}) and all possible directions (0–355°, with a step of 5°) of propagating atmospheric disturbances, and we introduce Proudman length, Pl, as:

$$Pl = \frac{L_{Fr\_crit}}{L_{tot}} \qquad (2)$$

where L_{Fr_crit} is the length of the path over which Froude number (Fr) is within the range $0.95 < Fr < 1.05$, and L_{tot} is the total path length spanning off the selected point towards the opposite shore in the direction of the incoming atmospheric disturbance, up to 150 km from a station. Froude number is defined as

$$Fr = \frac{u}{c} = \frac{u}{\sqrt{gh}} \qquad (3)$$

where u is the speed of the atmospheric disturbance, and c is the speed of long ocean waves (g is gravity acceleration, and h is sea depth). The larger the Proudman length, the stronger generation of meteotsunami waves through Proudman resonance is expected.

3. Results

3.1. General characteristics of short-period sea level oscillations

Representative examples of intense meteotsunamis together with air-pressure (for summer-type events) and wind (for winter-type events) measured at the nearest meteorological station are displayed in Figs. 2 and 3. For summer-type events (Fig. 2), meteotsunamis usually occur simultaneously with rapid changes in air pressure. For example, on 19 May 2014, a MCS moved over the Gulf of Bothnia from the south to the north along the coast, with air pressure jumps and simultaneous sea
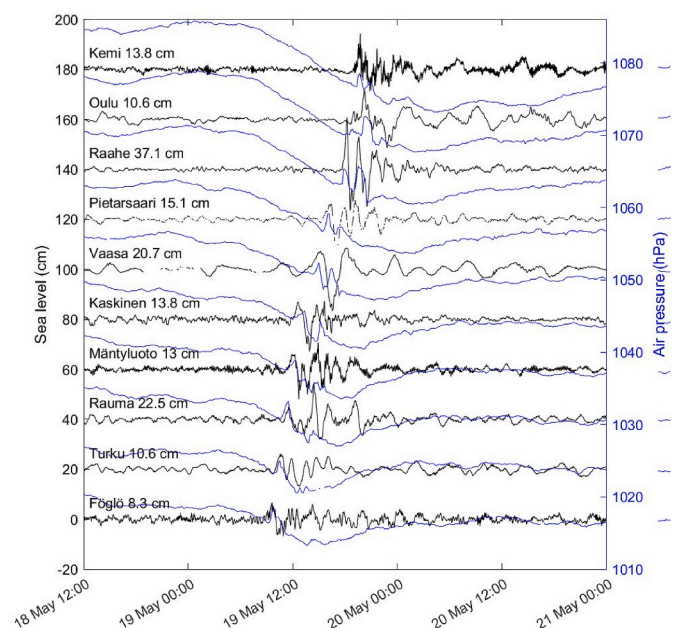

Fig. 2. Rapid sea level oscillations on 19 May 2014 in the Gulf of Bothnia (black) and air pressure at nearby coastal stations (blue). Maximum wave height at each station is indicated in the figure. The scales are for Föglö, other stations have been shifted vertically (+20 cm and +7 hPa per each successive station).
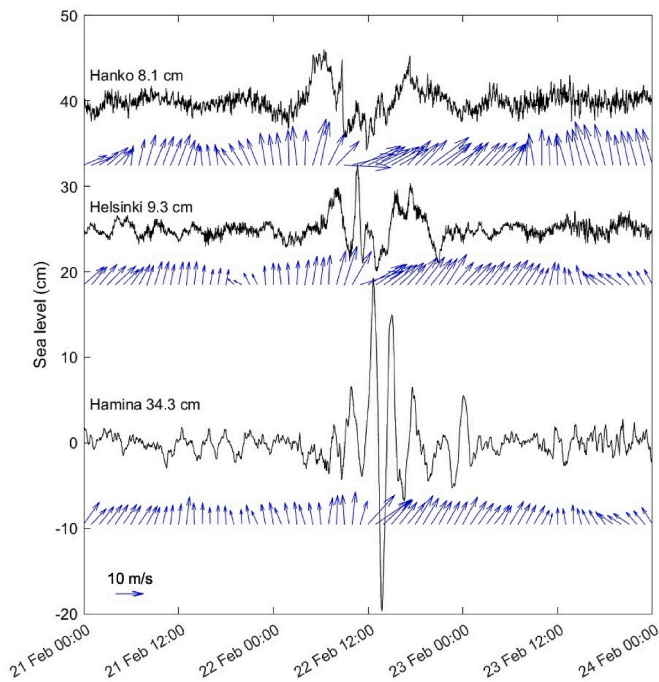
Fig. 3. Rapid sea level oscillations (black) on 22 Feb 2015 in the Gulf of Finland and wind vectors (black) every 1 h at nearby coastal stations. Maximum wave height at each station is indicated in the figure. The sea level scale is for Hamina, other stations have been shifted vertically (+25 cm for Helsinki and +40 cm for Hanko).

level oscillations (T < 6 h) of 10–40 cm recorded at tide gauges (Fig. 2), pointing to a clear link between air pressure and sea level oscillations. Herein, air pressure jumps refer to substantial changes in air pressure within a relatively short time interval. During the mentioned event the air pressure increased by up to 3.5 hPa in 30 min, and the maximum rate of air pressure change was 2 hPa/10 min. Such values are commonly found in other parts of the world during strongest meteotsunamis (e.g., Šepić et al., 2012; Rabinovich, 2020).

As an exemplary Gulf of Finland winter-type event, we choose the event on 22 February 2015 (Fig. 3), during which strong sea level oscillations are observed in Hamina (>30 cm of wave height). At all three examined stations, strong southerly winds (15–30 m s^{-1}) preceded the event. Then, the wind rapidly changed its direction to south-easterly–easterly (indicating a passage of a strong front) approximately simultaneously with the recorded meteotsunami. The change of the wind direction coincides with the air pressure minimum (not shown). As there is bathymetry-driven ringing of oscillations at some stations (e.g., Hamina), it cannot be precisely determined if the front itself or meso-scale convective systems around the front generated the high-frequency sea level oscillations.

To quantify the amplification of the sea level energy during strong high-frequency sea level oscillations, spectra of background oscillations and of oscillations recorded during the events of 19 May 2014 and 22 February 2015 were estimated (Fig. 4). Half-overlapping Kaiser windows of 720 min (12 h) length were used over: (i) the entire period (2004–2015) to estimate spectra of background oscillations and (iI) over 4-day intervals centred over the events to estimate event spectra (e.g., Thomson and Emery, 2014). The spectra at all stations and for both summer- and winter-type events indicate that energy of oscillations is increased during the events at periods longer than 10 min, with the increase being largest (up to 20 times larger compared to the background spectra) over periods of ~60–120 min for the chosen summer type event, and at even longer periods for the chosen winter-type event. Interestingly, only weak amplification or no amplification occurred over short periods (<10 min). Nonetheless, these are periods at which some

stations exhibit spectral peaks, indicating eigen oscillations of a harbour, bay, or channel (e.g., Rabinovich, 2009). At Turku, in particular, there are many significant spectral peaks, indicating that the tide gauge is situated in a complex morphological region.

The distribution of maximum and 95th percentile wave height as determined from the *Extreme wave heights dataset* along both the Gulf of Bothnia and the Gulf of Finland (Fig. 5) indicate that weaker oscillations are observed at stations which are located along the open coastline (e.g., Helsinki, Kaskinen, Mäntyluoto), and stronger oscillations are recorded at stations located in harbours, bays, or channels. The largest oscillations, both maximum and 95th percentile ones, occur at stations inside deep bays, like Hamina and Oulu. Largest differences between the 95th percentile and maximum wave heights are observed at Raahe and Hanko stations, both of which are located in shallow bays. This difference may indicate resonant processes, other than harbour resonance, along wider shelves, like stronger Proudman resonance over the shelf or generation of edge waves along the coast (e.g., Yankovsky, 2008).

When analysing seasonal changes of extreme high-frequency sea level oscillations (Fig. 6), specific patterns can be depicted. Both the maximum wave height, its 75th percentile and median at the northern stations (Oulu, Raahe, Pietarsaari) are reached between August and October. At some stations – like Raahe – maximum wave heights are quantified as outliers, i.e., having an exceptional occurrence. Positive outliers are defined as values which are greater than $q_3 + 1.5 (q_3 - q_1)$, where q_1 and q_3 are the 25th and 75th percentiles of the sample data, respectively. However, the extreme events occur over a prolonged period of year, from May to September, implying that weaker extremes are concentrated in late spring and early summer. For the rest of the Gulf of Bothnia, from Turku to Vaasa and in Kemi (which is open to long ocean waves coming from the south) and Helsinki, there is no clear seasonal distribution of the strongest high-frequency sea level oscillations, although more extreme events may be found during the colder part of the year, i.e., from October to January. For the southern stations prone to larger amplifications (Föglö, Hanko, Hamina), maximum heights of extreme waves are reached from May to December, with the largest number of extreme events both during the spring season (May–June) and the last months of the year (October–December). Such a variability in high-frequency sea level extremes is found in most of the ocean, pointing to local properties important for the generation of long ocean waves (Zemunik et al., 2022a). At most stations the minimum number of events is recorded from February to April, during the time when sea ice has the largest extension over the northern Baltic Sea.

3.2. Summer-type events

Short summaries of the recorded meteotsunamis and meteorological conditions during the analyzed summer-type events are presented in Tables 2 and 3. All events were accompanied by a cold or occluded front or a block of thunderstorms, often referred to as a mesoscale convective system (MCS), propagating over the sea with a typical speed of 20–25 m s^{-1}. MCSs are generally much larger than individual thunderstorms, having a horizontal dimension of over 100 km and lasting several hours (Houze Jr, 1993; Punkka and Bister, 2015; Williams et al., 2021). The highest recorded waves during the summer events ranged between 15 and 44 cm, depending on the event. Regarding wave heights, it should be noted that the heights measured by tide gauges do not necessarily reflect the maximum wave heights observed along the coast, as the waves may be locally amplified by coastal topography, particularly in numerous bays and harbours through harbour resonance (Miles and Munk, 1961; Rabinovich, 2009), surpassing the wave height of 1 m (Pellikka et al., 2014).

In Figs. 7a and 8a we show mean synoptic conditions during the Gulf of Bothnia summer-type events and synoptic conditions during the selected 19 May 2014 event. Mean conditions were obtained by averaging ERA-Interim synoptic fields of mean sea level pressure, temperature at 850 hPa, and geopotential and velocity at 500 hPa, at times
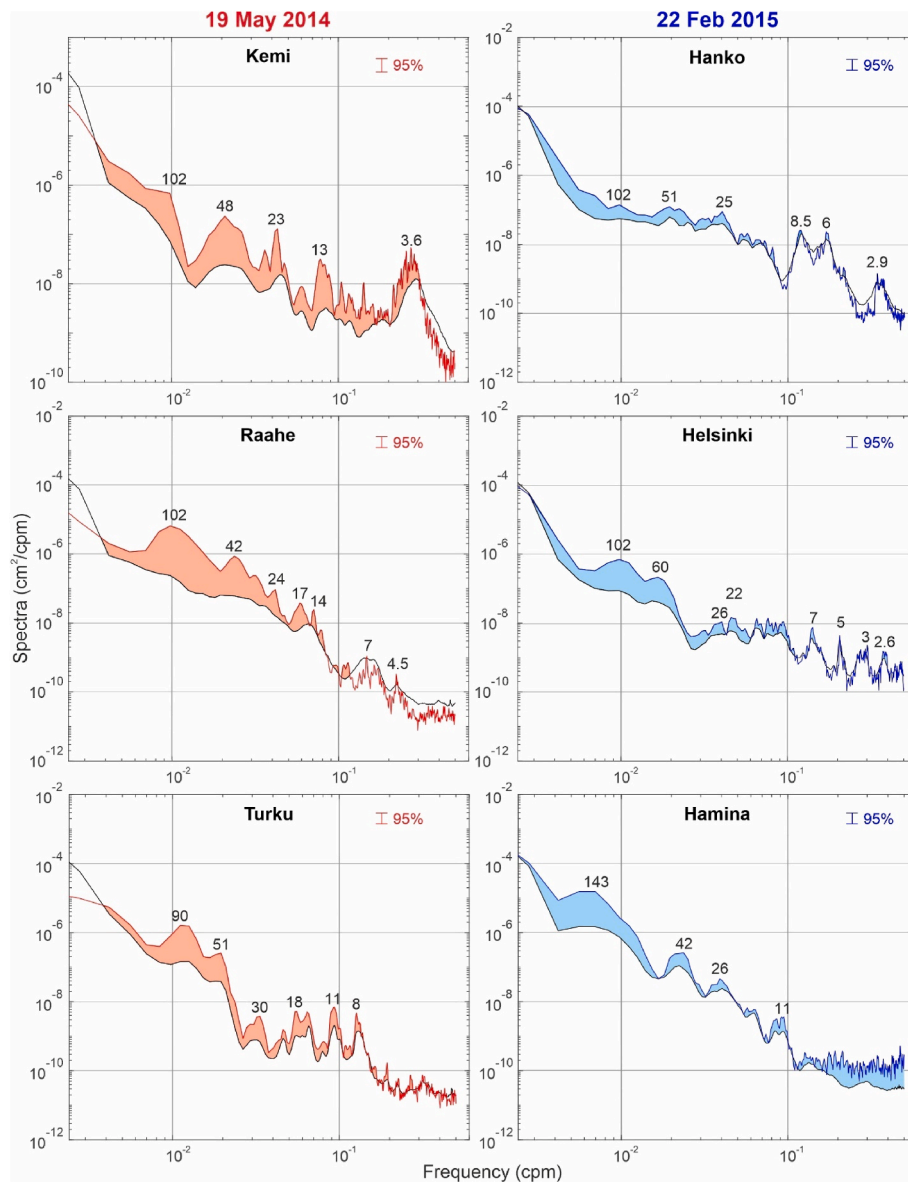
Fig. 4. Spectra of sea level oscillations at selected Finnish tide gauge stations during the background period and during the event of 15 May 2014 (left); the event of 22 February 2014 (right). Periods (in min) of strongest peaks are given. Background spectra are plotted with black lines, and event spectra with red and blue lines.

closest to event occurrences. Summer-type Gulf of Bothnia synoptic situations, during which high-frequency sea level oscillations appear, are characterized by (i) a surface high pressure area to the east (and less pronouncedly to the north) of the Baltic Sea and a weak surface low over the Baltic Sea and to the west of it, (ii) warm air advection east of the Baltic Sea at 850 hPa level, with the warm air originating from the Middle East, (iii) southern (occasionally southeastern or southwestern) winds of moderate speed at the 500 hPa level (mostly 15–20 m s^{-1} over the Gulf of Bothnia), (iv) inflow of dry air in the lower troposphere, between 600 and 950 hPa, and (v) level of minimum stability between 500 and 650 hPa. Radio-sounding data from Jokioinen (Figs. 9 and 10) show generally high CAPE, CINS and MLMR values during all events, with the respective average values of 828.2 J kg^{-1}, -152.0 J kg^{-1} and 12.4 g kg^{-1}. This reveals the existence of pronounced vertical convection during these events, which is also known to occur during the Mediterranean meteotsunamis (e.g., Jansà et al., 2007; Jansà and Ramis, 2021). No quantifiable correlations with wave heights are found, as the instabilities are always localized and therefore CAPE, CINS and MLMR normally have strong horizontal variability (Khairoutdinov and Randall, 2006). Nonetheless, comparison of wave height and CAPE, CINS, MLMR

data for a larger number of events could likely result with more reliable results.

As an illustrative event we chose the aforementioned 19 May 2014 Gulf of Bothnia summer event (Fig. 2; Fig. 4). During this event wave heights reached a maximum of 37 cm, and an air pressure jump was observed along the coast. Representative synoptic conditions are depicted in Fig. 8a, and the radio-sounding profile in Fig. 9. One can denote a local maximum of mid-troposphere winds over the Baltic Sea, advecting air towards the polar jet located at the latitude of 70–75°N. Warm air of the Middle East origin is advected towards the Baltic Sea in the low troposphere. A small area of unstable mid-troposphere air masses, overtopping areas slightly to the east of the Gulf of Bothnia, is present at the front of the jet stream local maximum, indicating a strong convergence region and a large potential for the development of mid- and upper troposphere MCSs (Machado et al., 1998).

The average synoptic setup of the Gulf of Finland summer-type events (Table 3, Fig. 7b) is similar to the one observed during the Gulf of Bothnia summer-type events. Nonetheless, over the Gulf of Finland some of the recorded meteotsunamis (three events) are associated with cold fronts which are moving generally from the west to the east, and
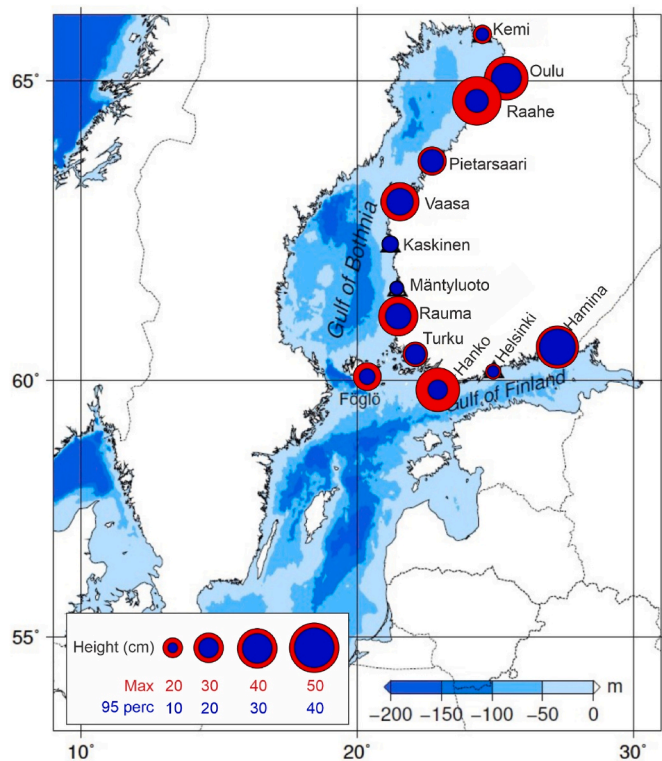
Fig. 5. Maximum (red circle) and 95th percentile (blue circle) wave heights at different tide gauges. The analysis is done only for events belonging to the *Extreme wave heights dataset*, i.e., for those events for which daily wave height surpassed 97.5th percentile of all daily wave heights at the respective station.

which are overtopped by a northward flow of warm air in the lower troposphere just south or southeast of the Gulf of Finland. Three events are associated with MCSs or gust fronts advancing from the south over the Gulf of Finland. The event of 29 July 2012, with the highest recorded CAPE values at Jokioinen (2112.1 J kg^{-1}), occurred at both the Gulf of Bothnia and the Gulf of Finland. Aside for this event, average CAPE, CINS and MLMR values were high during the majority of the Gulf of Finland summer-type events (Fig. 10), except during the event of 20 May 2014. However, the radio-sounding data preceding the event indicates the existence of instabilities in the atmosphere. For the Gulf of Finland cold front events, CAPE, CINS and MLMR values were substantially lower.

The representative synoptic summer-type Gulf of Finland event conditions are depicted for the event of 8 August 2010 (Figs. 8b and 9). Similarity with the synoptic setup of the 19 May 2014 Gulf of Bothnia event (Figs. 8a and 9) is evident. A northward mid-troposphere jet with a maximum wind speed of 18–26 m s^{-1} was present over the Gulf of Finland and to the south of it during the event. The lower troposphere advection of warm air from the Middle East was exceptional, with temperatures at 850 hPa surpassing 20°C and with distinct spatial temperature gradients overtopped by the mid-troposphere jet. The frontal part of the mid-troposphere jet was characterized by a broad region of unstable conditions, spreading over the whole Gulf of Finland and most of Finland (Fig. 8b).

3.3. Winter-type events

Short summaries of the recorded meteotsunamis and meteorological conditions during the analyzed winter-type events are presented in Tables 4 and 5. All Gulf of Bothnia events are related to cold fronts propagating over the sea and coming from the west-northwest-north (Fig. 11a, Fig. 12a). The speeds of weather systems appear to be smaller than during the summer events, typically 10–20 m s^{-1}; however,

they can occasionally be high as well (>30 m s^{-1} for the 11–12 October 2010 event). High-frequency sea level oscillations during the winter-type Gulf of Bothnia events mostly propagate from the north to the south, i.e. opposite to the summer-type events. Storm winds are frequently present. In all analyzed cases the sea was generally ice free, with some coastal ice recorded only in the northernmost parts of the Gulf of Bothnia (stations 1–2, Kemi and Oulu). Highest recorded waves at the tide gauges were up to 12–39 cm high during the winter-type events.

In the Gulf of Finland, all analysed winter events, except the event of 7 Mar 2015, were related to storms (Table 5). Typically, a deep low or extratropical cyclone is found moving from the west-northwest-north to the south-southeast-east (Figs. 11b and 12b), and sea level oscillations occur during the passage of the cold or occluded front of the low-pressure area. Typical speeds of weather systems are, similarly to the Gulf of Bothnia winter events, around 20 m s^{-1}. All of the Gulf of Finland events occurred during open sea conditions, with only some coastal ice in the easternmost parts of the gulf (station 13, Hamina).

In contrast to the MCS-related summer-type events for which rapid air pressure jumps are regularly observed, a passage of a low-pressure system of longer duration and a rapid change of winds has been frequently associated with the winter-type events. Some of the events are also associated with small pressure jumps (4 events out of 10 in the Gulf of Bothnia, 1 out of 7 in the Gulf of Finland).

Common synoptic conditions as revealed by the reanalysis (Figs. 11 and 12) and the radio-sounding (Fig. 13) data during the winter-type events are characterized for both the Gulf of Bothnia and the Gulf of Finland by (i) strong to very strong air pressure low or extratropical cyclone to the north of the area with intense pressure gradients over the northern Baltic Sea, (ii) warmer air in the lower troposphere to the south of Baltic advected from the Atlantic, and cold air advected from the polar areas with resulting strong thermal fronts overlying the Gulf of Bothnia and the Gulf of Finland, (iii) western (southwestern to north-western) winds of very high speeds, often higher than 40 m s^{-1}, at 500 hPa (Fig. 11), indicating that the central part of the mid-troposphere jet overlies the affected areas, and (v) usually unstable (or with low stability) lower atmospheric layers (from the surface up to 700 hPa).

Sounding data from Jokioinen for both the Gulf of Finland and the Gulf of Bothnia events (Fig. 14) show low CAPE, high CINS and low MLMR values, indicating that the vertical convection is low during the winter-type events. Mean CAPE, CINS and MLMR values for all winter-type Gulf of Bothnia and Gulf of Finland events (17 of them) are 7.2 J kg^{-1}, -18.0 J kg^{-1} and 4.1 g kg^{-1}, for CAPE and CINS one to two order of magnitude lower in absolute values than for the summer-type events.

As an example, synoptic conditions present over the area during the events of 6 January 2009 (the Gulf of Bothnia event) and of 22 February 2015 (the Gulf of Finland event) are depicted using both reanalysis (Fig. 12) and radio-sounding data (Fig. 13). The 6 January 2009 event was characterized by the north to the south propagation of a cold front (Table 4). At the time of the event, the speed of the eastward mid-troposphere jet was surpassing 22 m s^{-1} over most of the Gulf of Bothnia, advecting air of the Atlantic origin to the Baltic Sea. Surface winds, driven by a deep extratropical cyclone (MSLP of ~985 hPa) were also strong (up to 25 m s^{-1}). Synoptic analysis (Fig. 12a) reveals a south-westerly jet stream and advection of warmer air of Central Europe origin to the Gulf of Finland. The occluded front was associated with a deep extratropical cyclone located northward from the Baltic Sea, with the minimum air pressure of ca. 980 hPa.

4. Discussion and conclusions

On the Finnish coast, atmospheric conditions connected with meteotsunamis can be divided into summer and winter types, even though this classification does not strictly follow the seasonal division (May–Oct and Nov–Apr). Convincingly, it reflects the observed difference in synoptic conditions and in the genesis of the associated meteotsunamigenic disturbances, illustrated in Fig. 15.
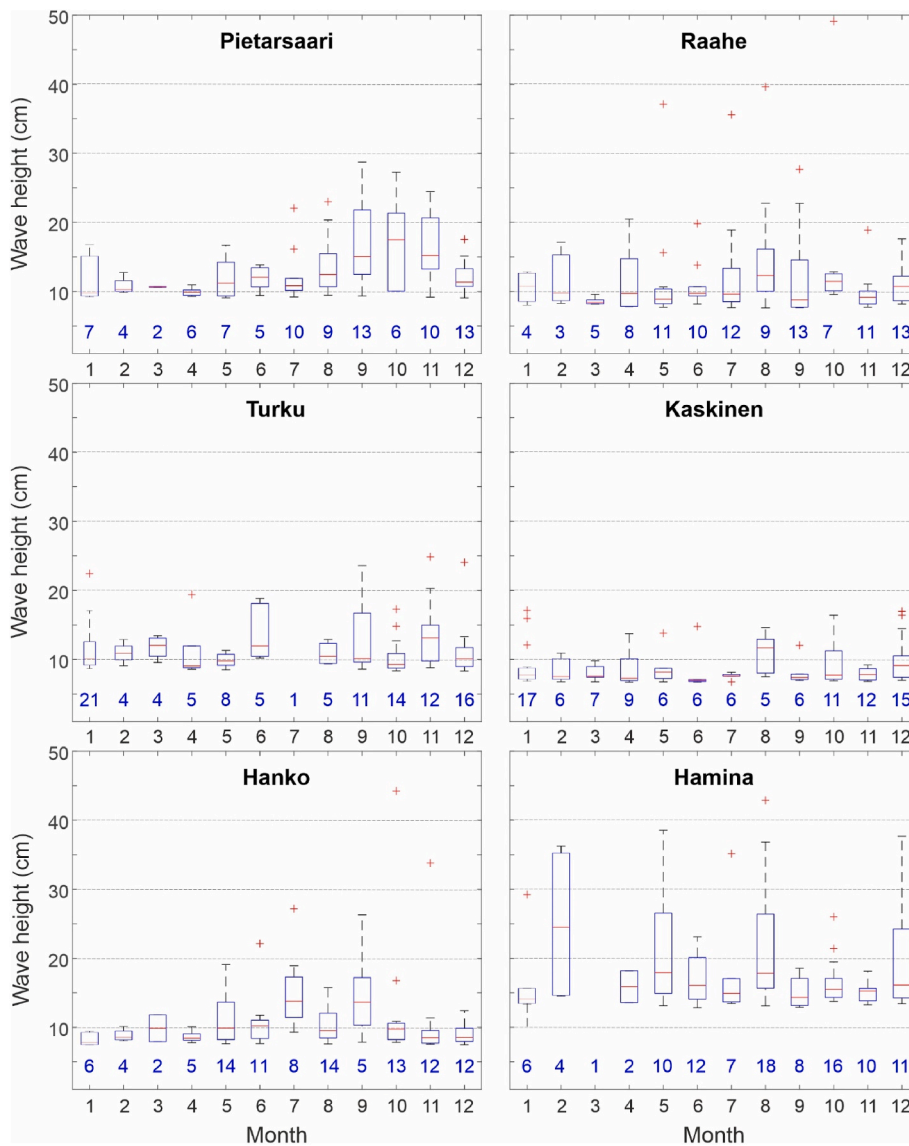
Fig. 6. Box-plots of the seasonal distribution of wave heights at selected Finnish tide gauge stations. Central red lines stand for median values, the top and bottom of boxes for the 25th and 75th percentile values, and the top and bottom of whiskers for minima and maxima; red crosses stand for outliers. The number of events per month is given with blue numbers. The analysis is done only for events belonging to the *Extreme wave heights dataset*, i.e., for those events for which daily wave height surpassed 97.5th percentile of all daily wave heights at the respective station.

Table 2
Analyzed summer-type events in the Gulf of Bothnia. Stations indicate the proportion of tide gauges where notable sea level oscillations were recorded (station numbers in parentheses, see Table 1); *hmax* is the maximum wave height (cm). Subsequent columns give atmospheric instability (assessed with the Richardson number), radio-sounding variables measured at Jokioinen (Convective Available Potential Energy CAPE in J kg^{-1}, Convective Inhibition CINS in J kg^{-1}, Mean Mixed Layer Mixing Ratio MLMR in g kg^{-1}), type of weather system related to the sea level event, presence of thunder (indicated with a lightning symbol), the estimated speed of the weather system (m s^{-1}), and a short description of the meteorological conditions.

Date	Stations	*hmax*	Insta-bility	CAPE /CINS /MLMR	Weather system	Thunder	Speed	Description
17–18 Aug 2008	*5/10* (4, 6–8, 10)	15	Yes	166.9/-155.3/12.1	Occluded Front		< 20	Thunder moving S to N, with air pressure variations
28–29 Jul 2010	*6/10* (1–5, 7)	36	Yes	194.4/-285.5/11.4	MCS		12–25	Several thunder areas moving S to N. Rapid air pressure variations
7–8 Aug 2010	*10/10* (1–10)	40	Yes	967.6/-282.7/13.5	MCS		20	Strong MCS moving over Åland late in the evening (with rapid air pressure variations of up to 4 hPa) and continuing northward. Another MCS moving over the northern Gulf of Bothnia in the morning
29–30 Jul 2012	*4/10* (7–10)	17	Some	2112.1/-1.9/15.0	MCS		20–25	Strong and wide MCS moving over the whole Baltic S to N. Air pressure variations along the Gulf of Bothnia coast from Turku to Vaasa. Same event observed also in the Gulf of Finland
19 May 2014	*9/10* (1–9)	37	Some	700.0/-34.5/9.8	MCS		20	MCS moving S to N over continent near the Gulf of Bothnia coast. Gust front and air pressure jump observed along the coast

Table 3
As in Table 2, but for the Gulf of Finland.

| Date	Stations	*hmax*	Insta-bility	CAPE /CINS /MLMR	Weather system	Thunder	Speed	Description
26 Aug 2005	*2/3* (11, 13)	37	Some	50.3/-135.2/9.2	Cold front + MCS		15–17	Cold front moving W to E over the Gulf of Finland, preceded by thunder. Air pressure minimum with a rapid jump at the time of the frontal passage
29 July 2010	*3/3* (11–13)	35	Yes	225.5/-236.0/11.4	Gust front + MCS		22	Gust front with thunder and an air pressure jump moving S to N over the Gulf of Finland from Estonia. Eyewitness observations of meteotsunamis at the coast (height up to >1 m; Pellikka et al. 2014)
8–9 Aug 2010	*2/3* (12–13)	43	Yes	158.2/-166.7/12.5	MCS		24	Strong MCS moving S to N over the Gulf of Finland, air pressure jumps. Eyewitness observations of meteotsunamis (Pellikka et al. 2014)
29 Jul 2012	*3/3* (11–13)	27	No	2112.1/-1.9/15.0	MCS		20–25	Strong and wide MCS moving over the whole Baltic S to N. Air pressure oscillations (up to 3 hPa) propagating on the Gulf of Finland coast from the west to the east. Same event observed also in the Gulf of Bothnia
27 Sep 2012	*2/3* (11, 13)	26	Some	4.7/-6.5/7.3	Cold front + MCS		20–25	Cold front from WSW to ENE, preceded by thunder. Pressure variations before the frontal passage, e.g. sudden pressure jump (2 hPa) in Hanko at 17 UTC, simultaneously with sea level oscillations
20 Oct 2012	*3/3* (11–13)	44	Yes	0.0/0.0/5.5	MCS + Cold front (later)		>20	Thunder moving over the sea from W to E. Rapid air pressure and wind speed variations after 16 UTC in the western Gulf of Finland, at 19 UTC in Helsinki
20 May 2014	*3/3* (11–13)	39	Some	0.8/-11.0/8.2	Gust front + MCS		25	Strong MCS formed south of the Gulf of Finland and propagated northward: air pressure variations especially in the eastern Gulf of Finland related to a gust front passage, coinciding with sea level oscillations. Another strong MCS over the eastern Gulf of Finland in the evening, accompanied by rapid pressure variations, again causing sea level oscillations
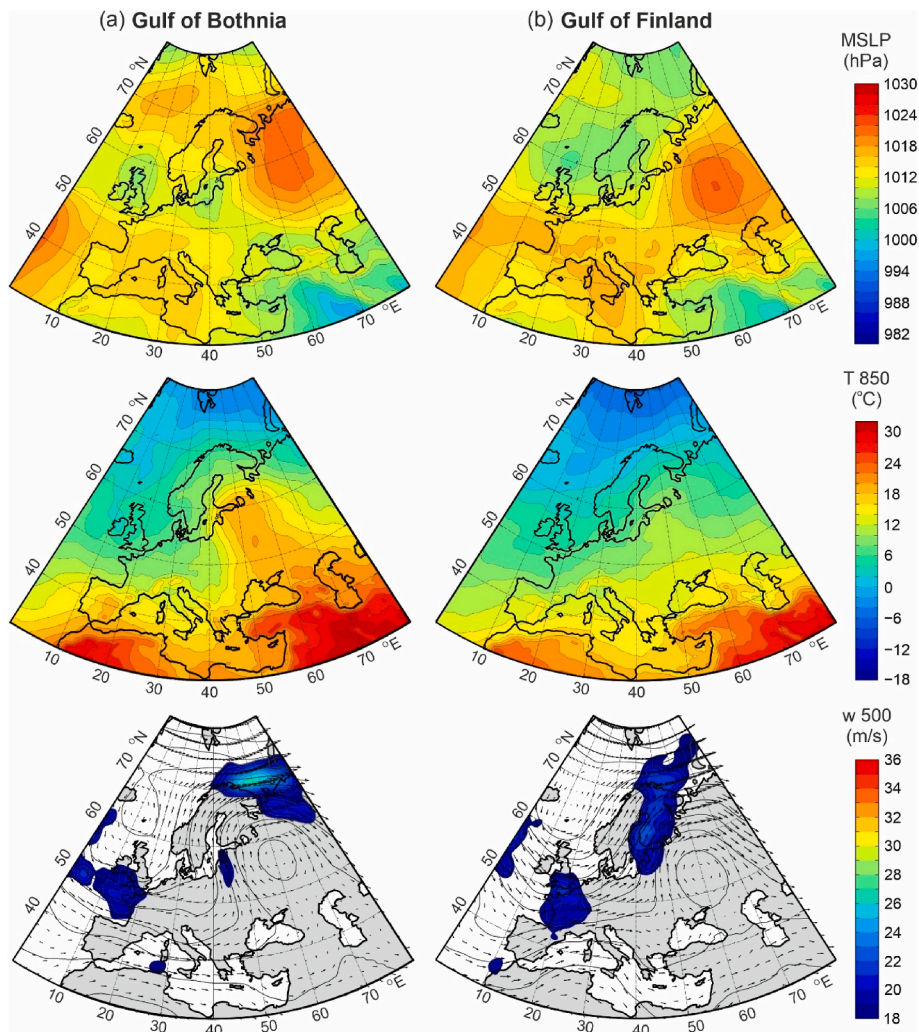
Fig. 7. Mean sea level pressure (*top*), temperature at 850 hPa (*middle*) and geopotential and winds at 500 hPa (*bottom*) over Europe during the summer-type sea level events over: (a) the Gulf of Bothnia and (b) the Gulf of Finland. Only winds faster than 18 m s⁻¹ are coloured in the bottom plot.
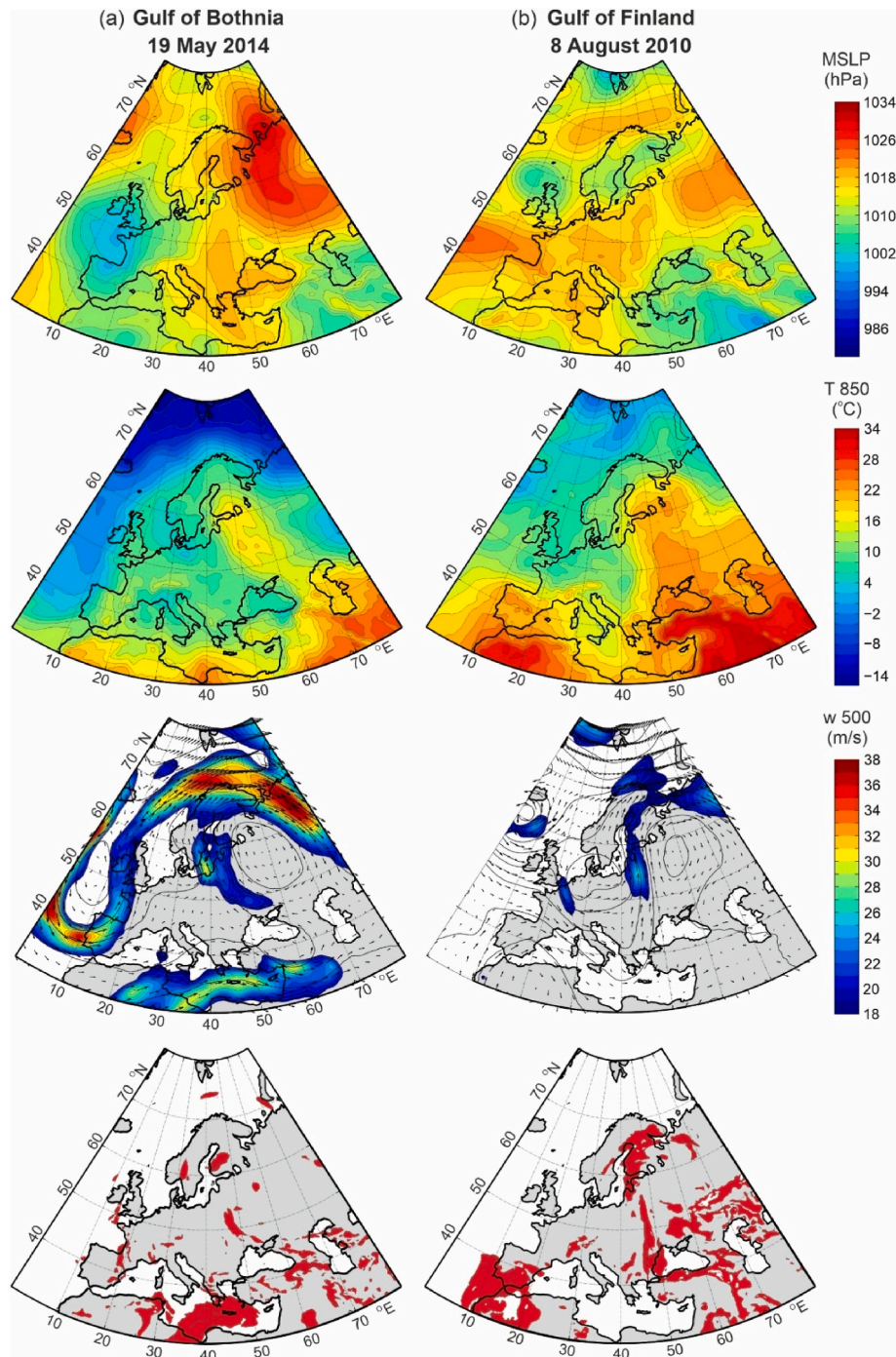
Fig. 8. ERA-Interim reanalysis fields of (*top*) mean sea level pressure; (2nd *row*) temperature at 850 hPa; (3rd *row*) geopotential and wind speed and direction at 500 hPa – only winds faster than 18 m s^{-1} are coloured; (*bottom*) minimum Richardson number between 400 and 700 hPa lower than 0.25 (in red), for: (a) 19 May 2014 at 12:00 UTC; (b) 8 August 2010 at 12:00 UTC.

Summer-type events are mostly associated with mesoscale convective systems (MCSs) propagating over the sea from the south to the north, occasionally conjoined with clear frontal structures (gust fronts). These events are accompanied with thunderstorms and rapid air pressure variations. Synoptic conditions during the events resemble conditions observed frequently during the Mediterranean meteotsunamis (Jansà and Ramis, 2021; Vilibić et al., 2021), for which wave-ducting or wave-CISK (Conditional Instability of the Second Kind) have been recognized as a dominant process of propagation of air pressure disturbances (Belušić et al., 2007; Monserrat and Thorpe, 1996; Horvath et al., 2018). These particularly refer to the existence of a

mid-troposphere jet overtopping a northward inflow of dry low troposphere air masses.

Punkka and Bister (2015) have studied the occurrence of MCSs in Finland. Their results show that MCSs are most common in July and August, and intense MCSs are very rare during winter. These events may be as extreme as the U.S. continental derechos (Punkka et al., 2006). However, non-intense MCSs occur almost daily in Finland during summer, but most of these are probably too weak and/or too slow for associated air pressure jumps to create significant meteotsunamis. Most of the MCSs are travelling towards the northeast (Punkka and Bister, 2015), followed by ~30% of northward or north-northwestward
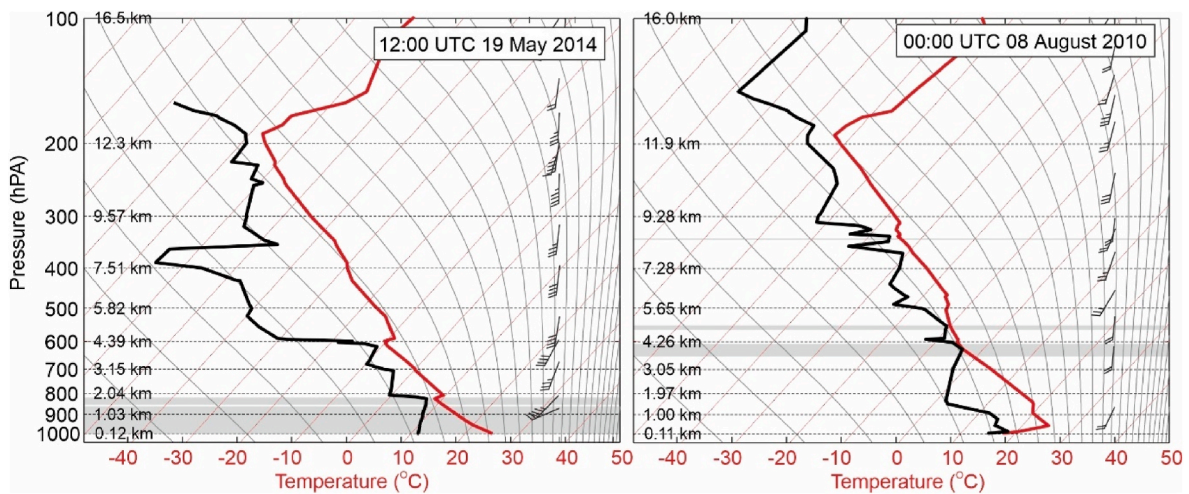
Fig. 9. Radio-sounding profiles measured at Jokioinen during: (*left*) the 19 May 2014 and (*right*) the 8 August 2010 events.
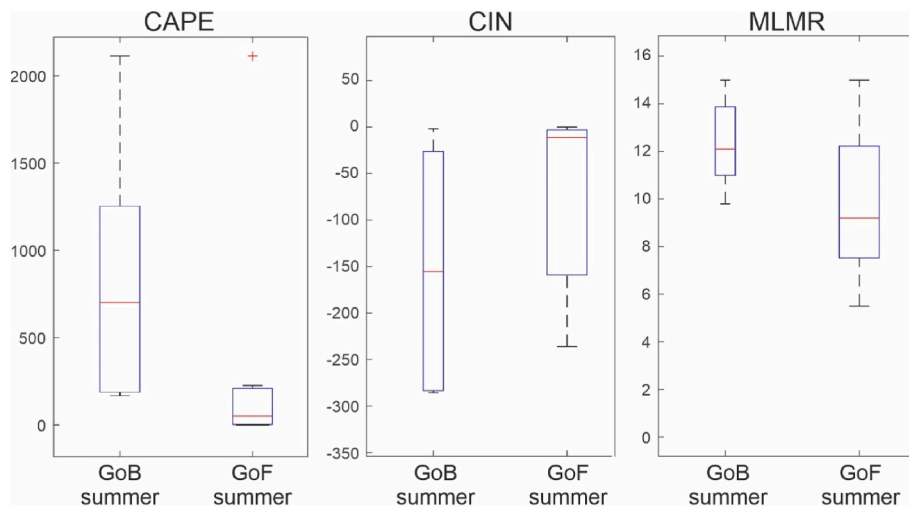

Fig. 10. Box-plot distribution of CAPE (J kg^{-1}), CIN (J kg^{-1}) and MLMR (g kg^{-1}) during summer-type events in the Gulf of Bothnia (GoB) and Gulf of Finland (GoF). Central red lines stand for median values, bottom and top of boxes for 25 and 75 percentile values and top and bottom of whiskers for minima and maxima; red crosses stand for outliers.

propagating MCSs.

In the Gulf of Bothnia, all of the recorded summer-type events were associated with MCSs, whereas in the Gulf of Finland, summer-type events were also generated by the eastward or northeastward propagation of frontal structures associated with advection of warm air to the south or the southeast from the Gulf of Finland. Presumably, such frontal structures, i.e., related surface air pressure disturbances, can generate meteotsunamis in the Gulf of Finland due to the orientation of the coastline which allows for higher amplification of the eastward advancing ocean waves, while the direction of preference is north-south in the Gulf of Bothnia. Conclusively, the occurrence and intensity of the summer-type Gulf of Finland and Gulf of Bothnia extreme high-frequency sea level oscillations are shaped by both weather systems and the bathymetry and orientation of the basins.

In winter, the studied meteotsunamis are exclusively related to the eastward to southward movement of frontal systems, mostly of cold fronts, and the associated rapid changes of high (usually stormy) wind speeds and directions. The winter-type events are conjoined with a pronounced mid-troposphere jet overtopping the northern Baltic Sea, with speeds frequently surpassing 40 m s^{-1} (Fig. 15b). Sea level oscillations during winter-type events generally propagate along coastline slower than during the summer-type events. An exceptional event is that

of 27 Dec 2011, when sea level oscillations were observed in the Gulf of Finland a few hours after the frontal passage. In this case, the direction of the front was clearly from the northwest to the southeast. It seems plausible that the observed sea level oscillations were reflections from the opposite shore of the Gulf of Finland – a process which is known to occur for long ocean waves (Vennell, 2010). The width of the Gulf of Finland is approximately 80 km and, if we estimate that ocean waves propagate with the shallow water phase speed calculated using the mean depth of the Gulf of Finland (19 m s^{-1}) and consider the propagation direction of the front and the orientation of the coastline, the crossing back and forth across the gulf takes roughly 2.5 h, similar to what was observed on 27 Dec 2011.

In Fig. 16 we show Proudman length estimated for two offshore locations ($\sim$5–10 km from the coast) close to Kaskinen and Hamina tide gauge stations. Kaskinen is chosen as a representative location for the Gulf of Bothnia, and Hamina as a representative location for the Gulf of Finland. We have chosen the offshore location, and not the tide gauge itself, as the algorithm for the estimation of Proudman length stops calculating the length when it "hits the coast" – thus, for the exact tide gauge locations, Proudman length for directions along the coast would be strongly underestimated by the algorithm. For both locations, estimated velocities of summer-type weather systems (mostly 20–30 m s^{-1};

Table 4
Analyzed winter-type events in the Gulf of Bothnia. Stations indicate the proportion of tide gauges where notable sea level oscillations were recorded (station numbers in parentheses, see Table 1); *hmax* is the maximum wave height (cm). Subsequent columns give atmospheric instability (assessed with the Richardson number), radio-sounding variables measured at Jokioinen (Convective Available Potential Energy CAPE in J kg^{-1}, Convective Inhibition CINS in J kg^{-1}, Mean Mixed Layer Mixing Ratio MLMR in g kg^{-1}), type of weather system related to the sea level event, the estimated speed of the weather system (in m s^{-1}), presence of ice (stations affected by ice are given in parentheses), and a short description of the meteorological conditions.

Date	Stations	*hmax*	Insta-bility	CAPE /CINS /MLMR	Weather system	Speed	Ice	Description
15 Nov 2004	*5/10* (1, 4–5, 9–10)	25	Some	5.9/-14.4/ 3.6	Cold front	10–15	No	Cold front moving N to S along the whole Gulf of Bothnia coast, followed by a trough and stormy winds in the evening. No rapid air pressure variations
16 Jan 2007	*6/10* (3–6, 8–9)	20	No	9.0/-1.6/ 4.4	Cold front	20–25	Some coastal ice in the northern Gulf of Bothnia (1–2, 5)	Cold front over the Gulf of Bothnia from W to E with high winds (occasional storm). Rise in air pressure after the frontal passage, no rapid variations
11 Apr 2007	*5/10* (4–5, 8–10)	33	No	0.0/0.0/ 2.7	Cold front	15	The northern Gulf of Bothnia partially ice-covered (1–5)	Cold front over the Gulf of Bothnia from NW to SE. Stronger sea level oscillations in the south, where the passage was marked by an air pressure jump and a rapid change in wind direction
29 Apr 2007	*4/10* (4–6, 8)	25	No	6.7/0.0/ 2.8	Cold front	<15	Ice in the northernmost Gulf of Bothnia (1–3)	Cold front from N to S along the coast, followed by an air pressure jump (1–2 hPa) except in the northernmost Gulf of Bothnia, where sea level oscillations are also weak
13 Feb 2008	*4/10* (2–4, 8)	17	No	3.3/-13.9/ 3.3	Cold front	15	A little ice on the coast (1–2, 5)	Cold front moving fast from NW to SE. Stormy winds from NW. No prominent air pressure oscillations
6 Jan 2009	*5/10* (5–9)	29	Some	0.0/0.0/ 2.7	Cold front	<10	Some coastal ice (1–9, esp. 1–2)	Cold front from N to S, arrived on the coast in the southern Gulf of Bothnia together with sea level oscillations. Rise in air pressure after the frontal passage, no rapid variations
11–12 Oct 2010	*5/10* (2, 5–8)	20	No	0.9/-155.3/ 12.1	Cold front	>30	No	Cold front moving N to S over the Gulf of Bothnia, with high winds of up to 26 m s^{-1}. Small air pressure jump after the frontal passage
4 June 2011	*5/10* (2–5, 10)	19	No	12.6/-61.2/6.6	Cold front	13–17	No	Cold front moving NW to SE over the Gulf of Bothnia, little thunder over continent. Air pressure minimum with a rapid jump at the time of the frontal passage. Eyewitness observation of a meteotsunami in Turku archipelago (Pellikka et al. 2014)
12–13 Dec 2013	*8/10* (3–10)	27	No	0.2/-13.9/ 3.7	Cold + occluded	20	Some coastal ice (1–7, esp. 1–2)	A deep low moved eastward causing a strong storm in the southern Finland, preceded by a cold front moving from NW to SE. A trough or occluded front arrived at the coast between 22 and 02 UTC, followed by NW storm. No rapid air pressure variations
23 May 2015	*6/10* (2–5, 8–9)	20	No	4.8/-13.4/ 3.8	Cold front	10–20	No	Cold front moving over the Gulf of Bothnia from W to E, followed by a storm in the northern Gulf of Bothnia. Rise in air pressure after the frontal passage, no rapid variations

Table 5
As in Table 4, but for the Gulf of Finland.

| Date	Stations	*hmax*	Insta-bility	CAPE /CINS /MLMR	Weather system	Speed	Ice	Description
9 Jan 2005	*3/3* (11–13)	29	No	0.0/0.0/3.5	Occluded front + storm	20	Very little (13)	A very deep low moved eastward causing a strong storm in Sweden and Estonia; stormy winds also in the southernmost Finland. The occluded front of the low moved over the Gulf of Finland from W to E causing record floods on the coast. Air pressure minimum after frontal passage, no rapid variations
15 Nov 2005	*3/3* (11–13)	16	No	25.6/-9.0/ 4.6	Cold front	22	No	Cold front related to a deep low moved over the Gulf of Finland from W to E. Stormy winds; no rapid changes in air pressure
20 Jan 2007	*3/3* (11–13)	14	No	3.9/0.0/2.3	Storm (south of Gulf of Finland)	20	No	A deep low moved from W to E south of Finland. SW storm in the southern Baltic Sea, in Finland steady easterly winds (10–15 m s^{-1}), no rapid air pressure variations
2–3 Feb 2008	*3/3* (11–13)	12	No	0.3/0.0/3.0	Cold front	15	Very little (13)	Cold front over the Gulf of Finland from W to E, shifting winds rapidly from SW to NW. Stormy winds in the southern Gulf of Bothnia. No rapid air pressure variations
27 Dec 2011	*2/3* (12–13)	38	Some	45.8/-21.9/ 3.5	Cold front	20–25	No	Two successive strong storms, followed by a cold front moving from NW to SE over the Gulf of Finland with a jump in air pressure. Strongest sea level oscillations occur several hours later, after 12 UTC
22 Feb 2015	*3/3* (11–13)	34	No	4.2/0.0/3.7	Trough or occluded front	20	Some coastal ice (13)	A low-pressure area propagating northeast over central Finland. A trough moving over the Gulf of Finland coast simultaneously with sea level oscillations, followed by a rise in air pressure and a brief storm from W
07 Mar 2015	*3/3* (11–13)	14	No	0.0/0.0/4.2	Warm	18–20	Some coastal ice (13)	A warm front moving W to E over the Gulf of Finland. Short pressure minimum during the passage of the front
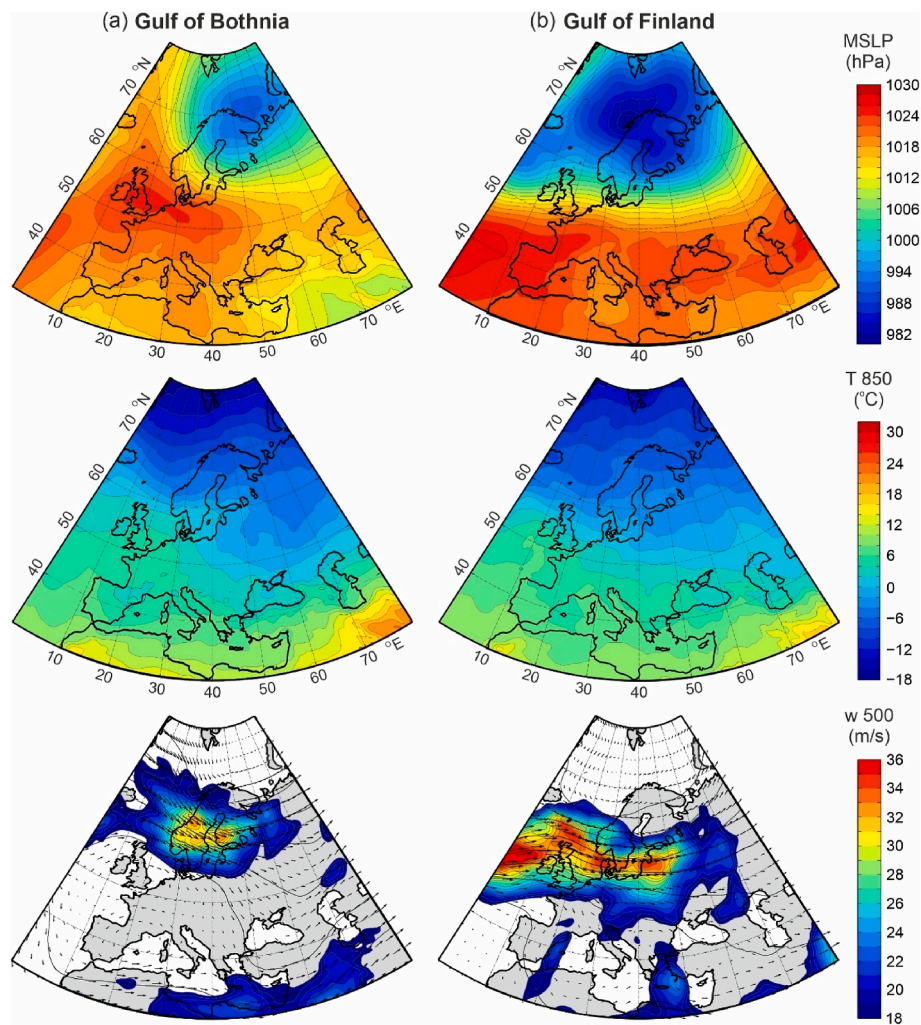
Fig. 11. Mean sea level pressure (*top*), temperature at 850 hPa (*middle*) and geopotential and winds at 500 hPa (*bottom*) over Europe during the winter-type sea level events over: (a) the Gulf of Bothnia and (b) Gulf of Finland. Only winds faster than 18 m s^{-1} are coloured in the bottom plot.

systems coming from the south) fall into velocity ranges for which strong Proudman resonance is expected (orange to red areas in Fig. 16; Proudman length >40%). Our analysis thus suggests that Proudman resonance is the main governing mechanism of the summer-type meteotsunamis.

On the contrary, estimated velocities of winter-type weather systems (mostly 10–20 m s^{-1}, systems coming from the north to the northwest), do not fall into velocity ranges for which strong Proudman resonance is supposed to occur (mostly bluish colours in Fig. 16; Proudman length <20%). This discrepancy points to any of the following: (1) these long ocean waves are not generated through Proudman resonance, but through other processes, possibly Greenspan resonance, or (2) the speed of frontal zones differs from the speed of atmospheric waves directly responsible for meteotsunamis, with the latter potentially generated through the convective activity in the fronts but then being separated from them and travelling freely from the source (as observed along the U.S. West Coast, Rabinovich et al., 2020); (3) the events which we have studied are indeed generated through Proudman resonance, but are not the strongest events which we can expect – for atmospheric disturbances propagating with velocities closer to resonant velocity, even stronger and more hazardous high-frequency sea level oscillations can be expected. Regardless of their generation mechanism over the open sea, the spatial distribution of maximum wave heights (Fig. 5) implies that long ocean waves are additionally strengthened through harbour resonance at locations within bays and harbours.

Regarding Greenspan resonance, for the zeroth mode, the speed of an edge wave in the southern Gulf of Bothnia and most of the Gulf of Finland, where the average slope of the shelf is around 0.003, is around 17 m s^{-1} for disturbances with periods of about 1 h (Ursell, 1952; Yankovsky, 2008) – matching closer lower velocities of winter weather systems. A way to quantify the role of both Proudman and Greenspan resonances, as well as their maximum impact, would be to conduct sensitivity modelling studies with varying speed and direction of the meteotsunamigenic disturbances (e.g., Šepić et al., 2016b).

It should be noted that some meteotsunami events of winter-type may be conjoined with an extensive storm surge or other processes, like the 9 January 2005 event in the Gulf of Finland (storm Gudrun) that resulted in record sea level heights and significant flooding damage (Suursaar et al., 2006). There is a resemblance of this event to, for example, the November 2019 flood of Venice during which high-frequency sea level oscillations occurred atop of a substantial storm surge (Ferrarin et al., 2021), or to the hurricane-generated coastal flooding embedding strong high-frequency sea level oscillations (Shi et al., 2020; Heidarzadeh and Rabinovich, 2021; Medvedev et al., 2022). Coastal floods in the Baltic Sea are a compound effect of several factors, including longer-period factors such as high water level in the Baltic Sea basin and seiche oscillations in the combined basin of the Gulf of Finland and the Baltic Proper (period ca. 24 h, Jonsson et al., 2008). In order to comprehend the true danger of extreme sea levels in the Baltic, it is thus essential to thoroughly analyse sea level processes occurring over
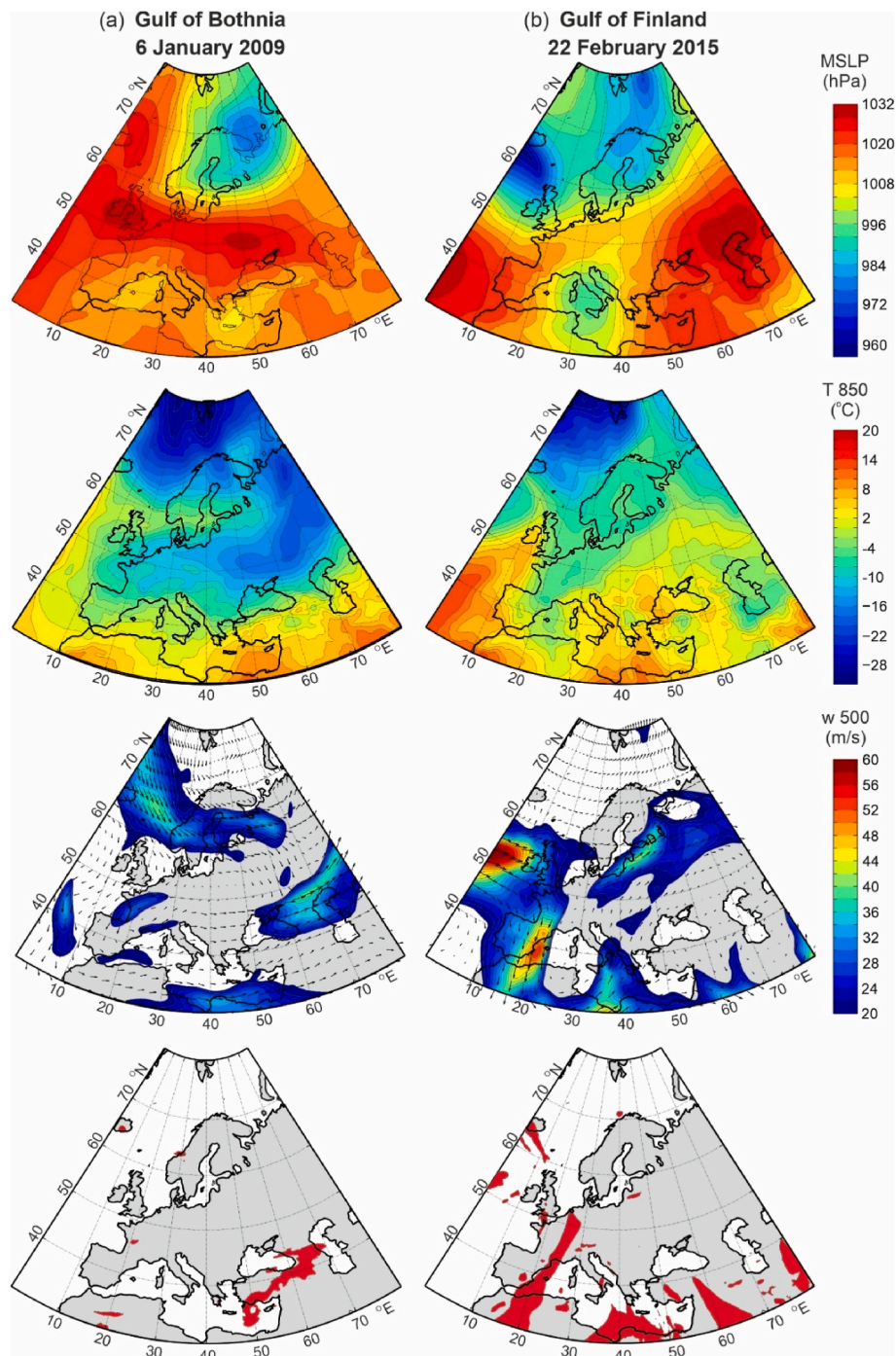
Fig. 12. ERA-Interim reanalysis fields of (*top*) mean sea level pressure; (2nd *row*) temperature at 850 hPa; (3rd *row*) geopotential and wind speed and direction at 500 hPa – only winds faster than 18 m s^{-1} are coloured; (*bottom*) minimum Richardson number between 400 and 700 hPa lower than 0.25 (in red), for: (a) 6 January 2009 at 12:00 UTC; (b) 22 February 2015 at 12:00 UTC.

various time scales, from seconds to millennia.

Research of the Mediterranean meteotsunamis (Šepić et al., 2009, 2015) implies that these events are occasionally associated with one another due to propagation of favourable synoptic patterns from one part of the Mediterranean to another. We were interested whether something like this holds for the Finnish high-frequency sea level oscillations as well. Thus, we have examined available literature on other European events to look for possible matching. We found no matching events between the United Kingdom and Finnish events (neither by looking at herein analysed events nor by looking at events analysed by Pellikka et al., 2020) in published literature (Haslett et al., 2009).

However, the event of 19–20 May 2014 appears to be conjoined to a smaller meteotsunami recorded along the northern European coast during 18–22 May 2014, during which maximum wave heights reached 73 cm in Boulogne (Belgium) (Lewis et al., 2022). We further examined the global meteotsunami catalogue discussed by Gusiakov (2021) but, again, found no matching events over the northern Europe and Finland. Interestingly, when we shifted our focus to the more distant Mediterranean, we found a couple of strong high-frequency sea level oscillation events at the Adriatic Sea and the Baltic, which appear to be associated to the same synoptic system. The first of these is the winter-type event of 20 January 2007 (Table 5, Gulf of Finland) which was associated with an
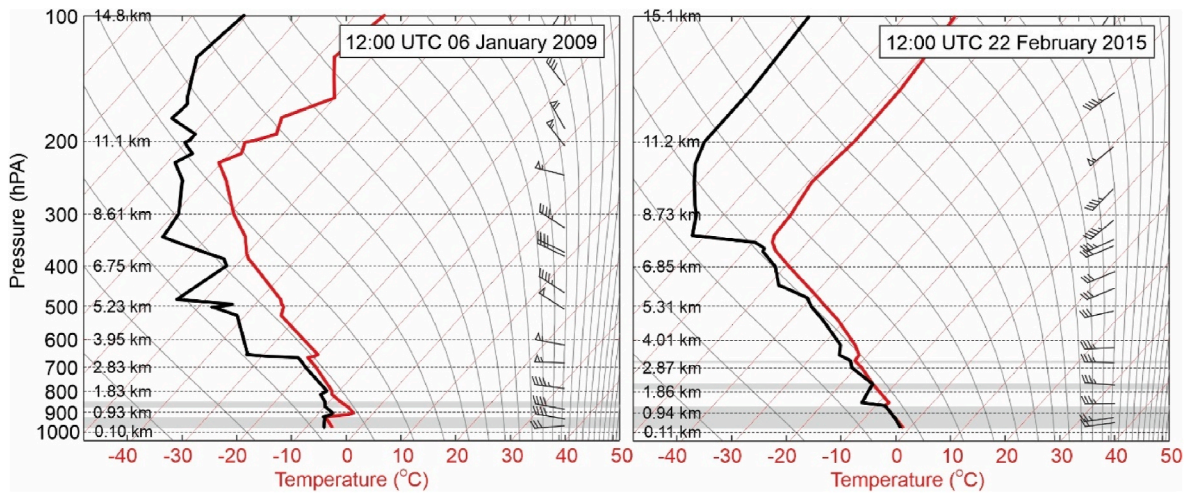
Fig. 13. Radio-sounding profiles measured at Jokioinen during: (*left*) 6 January 2009 and (*right*) 22 February 2015 events.
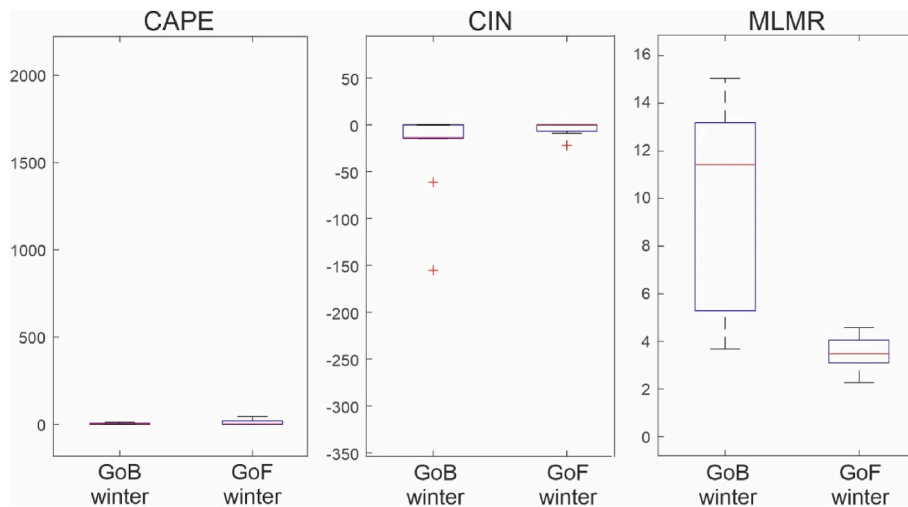

Fig. 14. Box-plot distribution of CAPE (J kg^{-1}), CIN (J kg^{-1}) and MLMR (g kg^{-1}) during winter-type events in the Gulf of Bothnia (GoB) and Gulf of Finland (GoF). Central red lines stand for median values, bottom and top of boxes for 25 and 75 percentile values and top and bottom of whiskers for minima and maxima; red crosses stand for outliers.

upper air deep trough and cold air advection from the north. Within the next few days, the trough and advection spread to the south, reaching the Adriatic Sea by 23 January 2007 – at this time intense high-frequency sea level oscillations were recorded in the northern and middle Adriatic (Krešimir Ruić, personal communication). On the contrary, on 15 August 2008, a strong meteotsunami was observed in the middle Adriatic (Vilibić and Šepić, 2009), and a few days later exceptional high-frequency sea level oscillations were recorded in the Gulf of Bothnia (17–18 August 2008; Table 2). Both events were associated with a characteristic synoptic system which propagated from the southern Europe towards the northern Europe and which, typically, included advection of warm air of African origin at lower troposphere, and a strong mid-troposphere jet stream. Our characteristic synoptic setting (Fig. 15) suggests that summer-type Finnish events might be connected to the Black Sea events – since the synoptic pattern associated to Finnish meteotsunamis seems to occasionally be present over the Black Sea at the same time (e.g., Fig. 8b). However, due to the lack of data for this area (only two known meteotsunamis occurred there; Vilibić et al., 2010; Rabinovich, 2020), we are not able to make a proper assessment.

Finally, we discuss the possibility of using synoptic conditions and synoptic indices to quantify the relationship between synoptic variables and high-frequency sea level oscillations along the Finnish coast, and to

eventually forecast these oscillations. A similar approach has been suggested for the Balearic Islands (Šepić et al., 2016b; Vilibić et al., 2018). However, the Balearic meteotsunamis appear to occur under one set of very specific synoptic conditions which prevails during the summer months (Jansà and Ramis, 2021; Vilibić et al., 2021); whereas the herein discussed Finnish events appear under two different synoptic settings. Zemunik et al. (2022b) tested correlations between synoptic variables and high-frequency sea level oscillations over the World: for the Baltic Sea, these correlations are approximately two times lower than for the Mediterranean Sea. Indicatively, a more elaborate approach should be used to construct Finnish meteotsunami synoptic indices – this approach should account for the difference between summer-type and winter-type events. Such a model, that may also embed a pattern-recognition technique, may be applied to qualitatively forecast extreme high-frequency sea level oscillations at the Baltic Sea.

To conclude, there are several novelties in this study not accounted for in the previous research: (1) the existing knowledge on the Baltic meteotsunamis was based on either eyewitness reports or historical 15-min data collected at three Gulf of Finland stations (Pellikka et al., 2020) – in our study, these analyses are supplemented by adding the Gulf of Bothnia stations, expanding slightly the period of data availability (up to 2015), and by using 1-min data; (2) we classified the northern Baltic
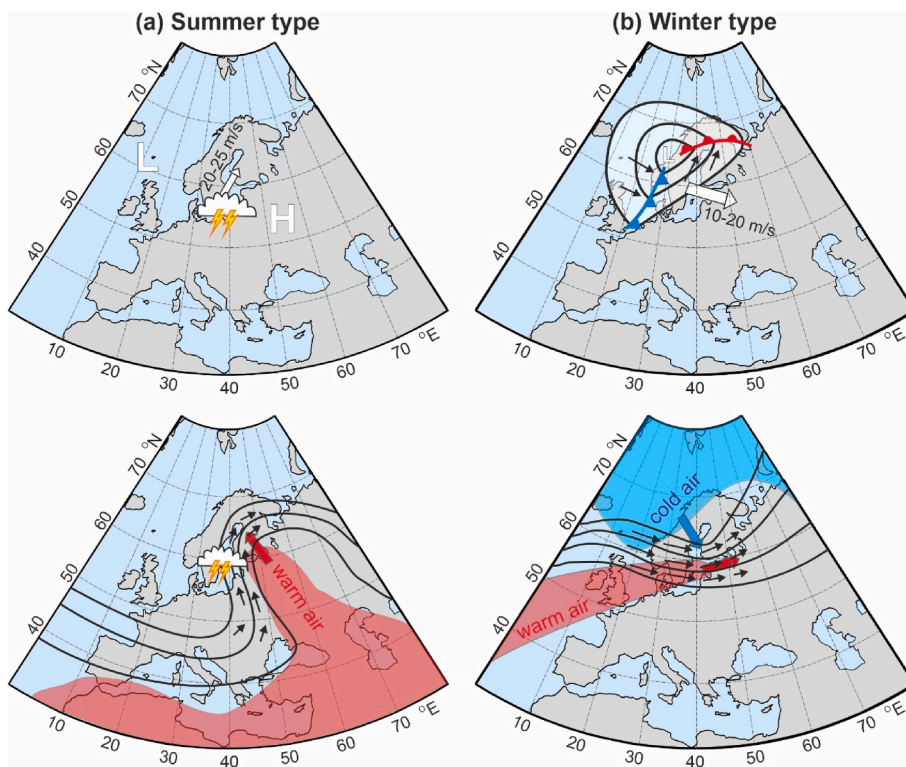
Fig. 15. An illustration of: (*top*) dominant surface and (*bottom*) low and mid-tropospheric atmospheric conditions and weather systems observed during extreme meteotsunamis in the northern Baltic Sea during (a) MCS-driven summer-type events and (b) winter-type events associated with cold fronts. Red (blue) shaded areas in bottom plots indicate advection of warm (cold) air at t850 hPa level; black lines (geopotential) and black arrows (wind) mark the position of the 500 hPa jet stream. Filled arrows mark the general direction of movement of MCSs, extratropical cyclones, and warm and cold air advection, with average speed of movement given for MCSs and extratropical cyclones.
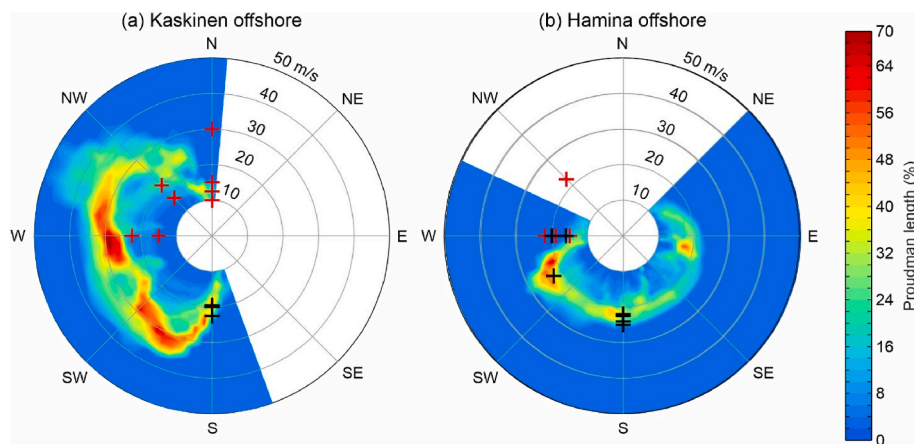
Fig. 16. Proudman length estimated for: (a) a representative Gulf of Bothnia location (Kaskinen offshore), and (b) a representative Gulf of Finland location (Hamina offshore). Crosses stand for estimated velocities of (*black*) summer weather systems (Tables 2 and 3); (*red*) winter weather systems (Tables 4 and 5) associated with selected events.

meteotsunamis with respect to synoptic conditions, which has so far been only done for the western Mediterranean (Šepić et al., 2016b; Jansà and Ramis, 2021) and the North Sea (Williams et al., 2021), (3) we performed an initial assessment of the underlying generation processes in both the atmosphere and the ocean. For going deeper into the processes, atmosphere-ocean coupled numerical modelling at high resolutions should be performed (e.g., Anderson et al., 2015; Denamiel et al., 2019; Robertson et al., 2022). With established connection at the synoptic scale (through a synoptic index) and mesoscale (through high-resolution atmosphere-ocean model), a forecast system may be foreseen as feasible, like one for the Balearic Islands (Jansà and Ramis, 2021), providing a valuable input for mitigating coastal hazards and increasing safety of navigation in coastal regions (Ozsoy et al., 2016).

Credit author statement

Havu Pellikka: Conceptualization, Methodology, Formal analysis, Investigation, Writing – Original Draft, Visualization; Funding acquisition; **Jadranka Šepić:** Conceptualization, Methodology, Formal analysis, Investigation, Writing – Review & Editing, Visualization; Funding acquisition; **Ilari Lehtonen:** Conceptualization, Methodology, Formal analysis, Writing – Review & Editing; **Ivica Vilibić:** Conceptualization, Methodology, Writing – Review & Editing.

Declaration of competing interest

The authors declare that they have no known competing financial interests or personal relationships that could have appeared to influence the work reported in this paper.

Data availability

Acknowledgements

References

Anderson, E.J., Bechle, A.J., Wu, C.H., Schwab, D.J., Mann, G.E., Lombardy, K.A., 2015. Reconstruction of a meteotsunami in Lake Erie on 27 May 2012: roles of atmospheric conditions on hydrodynamic response in enclosed basins. J. Geophys. Res. Oceans 120, 8020–8038. https://doi.org/10.1002/2015JC010883.

Averkiev, A.S., Klevannyy, K.A., 2010. A case study of the impact of cyclonic trajectories on sea-level extremes in the Gulf of Finland. Continent. Shelf Res. 30 (6), 707–714. https://doi.org/10.1016/j.csr.2009.10.010.

Belušić, D., Grisogono, B., Bencetić Klaić, Z., 2007. Atmospheric origin of the devastating coupled air-sea event in the east Adriatic. J. Geophys. Res. 112 https://doi.org/10.1029/2006JD008204.

Credner, R., 1889. Über den "Seebär" der westlichen Ostsee vom 16/17.Mai 1888. III Jahresbericht der Geographischen Gesellschaft zu Greifswald 1886–1889, pp. 57–96.

Dee, D., Uppala, S., Simmons, A., Berrisford, P., Poli, P., Kobayashi, S., Andrae, U., Balmaseda, M., Balsamo, G., Bauer, P., Bechtold, P., Beljaars, A.C.M., van de Berg, L., Bidlot, J., Bormann, N., Delsol, C., Dragani, R., Fuentes, M., Geer, A.J., Haimberger, L., Healy, S.B., Hersbach, H., Hólm, E.V., Isaksen, L., Kållberg, P., Köhler, M., Matricardi, M., McNally, A.P., Monge-Sanz, B.M., Morcrette, J.-J., Park, B.-K., Peubey, C., de Rosnay, P., Tavolato, C., Thépaut, J.-N., Vitart, F., 2011. The ERA-Interim reanalysis: configuration and performance of the data assimilation system. Q. J. R. Meteorol. Soc. 137, 553–597. https://doi.org/10.1002/qj.828.

Defant, A., 1961. Physical Oceanography, II. Pergamon Press.

Denamiel, C., Šepić, J., Ivanković, D., Vilibić, I., 2019. The Adriatic Sea and coast modelling suite: evaluation of the meteotsunami forecast component. Ocean Model. 135, 71–93. https://doi.org/10.1016/j.ocemod.2019.02.003.

Doss, B., 1906. Über ostbaltische Seebären. Gerlands Beiträge zur Geophysik 8, 367–399.

Durran, D.R., Klemp, J.B., 1982. On the effects of moisture on the Brunt-Väisälä frequency. J. Atmos. Sci. 39, 2152–2158. https://doi.org/10.1175/1520-0469(1982)039<2152:OTEOMO>2.0.CO;2.

Dusek, G., DiVeglio, C., Licate, L., Heilman, L., Kirk, K., Paternostro, C., Miller, A., 2019. A meteotsunami climatology along the U.S. East Coast. Bull. Am. Meteorol. Soc. 100, 1329–1345. https://doi.org/10.1175/BAMS-D-18-0206.1.

Ferrarin, F., Bajo, M., Benetazzo, A., Cavaleri, L., Chiggiato, J., Davison, S., Davolio, S., Lionello, P., Orlić, M., Umgiesser, G., 2021. Local and large-scale controls of the exceptional Venice floods of November 2019. Prog. Oceanogr. 197, 102628 https://doi.org/10.1016/j.pocean.2021.102628.

Greenspan, H.P., 1956. The generation of edge waves by moving pressure disturbances. J. Fluid Mech. 1, 574–592. https://doi.org/10.1017/S002211205600038X.

Gusiakov, V.K., 2021. Meteotsunamis at global scale: problems of event identification, parameterization and cataloguing. Nat. Hazards 106, 1105–1123. https://doi.org/10.1007/s11069-020-04230-2.

Haslett, S.K., Mellor, H.E., Bryant, E.A., 2009. Meteo-tsunami hazard associated with summer thunderstorms in the United Kingdom. Phys. Chem. Earth 34, 1016–1022. https://doi.org/10.1016/j.pce.2009.10.005.

Heidarzadeh, M., Rabinovich, A.B., 2021. Combined hazard of typhoon-generated meteorological tsunamis and storm surges along the coast of Japan. Nat. Hazards 106, 1639–1672. https://doi.org/10.1007/s11069-020-04448-0.

Heidarzadeh, M., Šepić, J., Rabinovich, A., Allahyar, M., Soltanpour, A., Tavakoli, F., 2020. Meteorological tsunami of 19 March 2017 in the Persian Gulf: observations and analyses. Pure Appl. Geophys. 177, 1231–1259. https://doi.org/10.1007/s00024-019-02263-8.

Horvath, K., Šepić, J., Telišman Prtenjak, M., 2018. Atmospheric forcing conducive for the Adriatic 25 June 2014 meteotsunami event. Pure Appl. Geophys. 175, 3817–3837. https://doi.org/10.1007/s00024-018-1902-1.

Houze Jr., R.A., 1993. Cloud Dynamics. Academic Press.

Jansà, A., Ramis, C., 2021. The Balearic rissaga: from pioneering research to present-day knowledge. Nat. Hazards 106, 1269–1297. https://doi.org/10.1007/s11069-020-04221-3.

Jansà, A., Monserrat, S., Gomis, D., 2007. The rissaga of 15 June 2006 in Ciutadella (Menorca), a meteorological tsunami. Adv. Geosci. 12, 1–4.

Jonsson, B., Doos, K., Nycander, J., Lundberg, P., 2008. Standing waves in the Gulf of Finland and their relationship to the basin-wide Baltic seiches. J. Geophys. Res. Oceans 113, C03004. https://doi.org/10.1029/2006JC003862.

Khairoutdinov, M., Randall, D., 2006. High-resolution simulation of shallow-to-deep convection transition over land. J. Atmos. Sci. 63, 3421–3436. https://doi.org/10.1175/JAS3810.1.

Leppäranta, M., Myrberg, K., 2009. Physical Oceanography of the Baltic Sea. Springer Science & Business Media.

Lewis, C., Smyth, T., Williams, D., Neumann, J., Cloke, H., 2022. Meteotsunami in the United Kingdom: the hidden hazard. EGUsphere. https://doi.org/10.5194/egusphere-2022-1145. Submitted for publication.

Machado, L.A.T., Rossow, W.B., Guedes, R.L., Walker, A.W., 1998. Life cycle variations of mesoscale convective systems over the Americas. Mon. Weather Rev. 126, 1630–1654. https://doi.org/10.1175/1520-0493(1998)126<1630:LCVOMC>2.0.CO;2.

Mäkelä, A., Enno, S.E., Haapalainen, J., 2014. Nordic lightning information system: thunderstorm climate of northern Europe for the period 2002–2011. Atmos. Res. 139 (Supplement C), 46–61. https://doi.org/10.1016/j.atmosres.2014.01.008.

Marchenko, A.V., Morozov, E.G., 2016. Surface manifestations of the waves in the ocean covered with ice. Russ. J. Earth Sci. 16, ES1001. https://doi.org/10.2205/2016ES000561.

Medvedev, I., Rabinovich, A., Kulikov, E., 2013. Tidal oscillations in the Baltic Sea. Oceanology 53 (5), 526–538.

Medvedev, I., Rabinovich, A.B., Šepić, J., 2022. Destructive coastal sea level oscillations generated by Typhoon Maysak in the Sea of Japan in September 2020. Sci. Rep. 12, 12189 https://doi.org/10.1038/s41598-022-12189-2.

Meissner, O., 1924. Zur Frage nach der Entstehung der Seebären. Ann. Hydrogr. Marit. Meteorol. 52, 14–15.

Miles, J., Munk, W., 1961. Harbor paradox. J. Waterways Harbors Div. ASCE 87, 111–132. https://doi.org/10.1061/JWHEAU.0000223.

Monserrat, S., Thorpe, A.J., 1996. Use of ducting theory in an observed case of gravity waves. J. Atmos. Sci. 53, 1724–1736. https://doi.org/10.1175/1520-0469(1996)053<1724:UODTIA>2.0.CO;2.

Monserrat, S., Vilibić, I., Rabinovich, A., 2006. Meteotsunamis: atmospherically induced destructive ocean waves in the tsunami frequency band. Nat. Hazards Earth Syst. Sci. 6, 1035–1051. https://doi.org/10.5194/nhess-6-1035-2006.

Orlić, M., 2015. The first attempt at cataloguing tsunami-like waves of meteorological origin in Croatian coastal waters. Acta Adriat. 56 (1), 83–96. http://jadran.izor.hr/acta/pdf/56_1_pdf/56_1_4.pdf.

Ozsoy, O., Haigh, I.D., Wadey, M.P., Nicholls, R.J., Wells, N.C., 2016. High-frequency sea level variations and implications for coastal flooding: a case study of the Solent, UK. Continent. Shelf Res. 122, 1–13. https://doi.org/10.1016/j.csr.2016.03.021.

Pawlowicz, R., Beardsley, B., Lentz, S., 2002. Classical tidal harmonic analysis including error estimates in MATLAB using T TIDE. Comput. Geosci. 28, 929–937. https://doi.org/10.1016/S0098-3004(02)00013-4.

Pellikka, H., Rauhala, J., Kahma, K.K., Stipa, T., Boman, H., Kangas, A., 2014. Recent observations of meteotsunamis on the Finnish coast. Nat. Hazards 74, 197–215. https://doi.org/10.1007/s11069-014-1150-3.

Pellikka, H., Laurila, T.K., Boman, H., Karjalainen, A., Björkqvist, J.-V., Kahma, K.K., 2020. Meteotsunami occurrence in the Gulf of Finland over the past century. Nat. Hazards Earth Syst. Sci. 20, 2535–2546. https://doi.org/10.5194/nhess-20-2535-2020.

Plougonven, R., Zhang, F., 2014. Internal gravity waves from atmospheric jets and fronts. Rev. Geophys. 52, 33–76. https://doi.org/10.1002/2012RG000419.

Proudman, J., 1929. The effects on the sea of changes in atmospheric pressure. Monthly Notices of the Royal Astronomical Society Geophysical Supplement 2 (4), 197–209. https://doi.org/10.1111/j.1365-246X.1929.tb05408.x.

Punkka, A.J., Bister, M., 2015. Mesoscale convective systems and their synoptic-scale environment in Finland. Weather Forecast. 30, 182–196. https://doi.org/10.1175/WAF-D-13-00146.1.

Punkka, A.J., Teittinen, J., Johns, R.H., 2006. Synoptic and mesoscale analysis of a high-latitude derecho-severe thunderstorm outbreak in Finland on 5 July 2020. Weather Forecast. 21, 752–763. https://doi.org/10.1175/WAF953.1.

Rabinovich, A.B., 2009. Seiches and harbour oscillations. In: Kim, Y.C. (Ed.), Handbook of Coastal and Ocean Engineering, 193–236. World Scientific, Singapore. https://doi.org/10.1142/9789812819307_0009.

Rabinovich, A.B., 2020. Twenty-seven years of progress in the science of meteorological tsunamis following the 1992 Daytona Beach event. Pure Appl. Geophys. 177, 1193–1230. https://doi.org/10.1007/s00024-019-02349-3.

Rabinovich, A.B., Monserrat, S., 1996. Meteorological tsunamis near the Balearic and Kuril Islands: descriptive and statistical analysis. Nat. Hazards 13, 55–90.

Rabinovich, A.B., Šepić, J., Thomson, R.E., 2020. The meteorological tsunami of 1 November 2010 in the southern Strait of Georgia: a case study. Nat. Hazards 106, 1503–1544. https://doi.org/10.1007/s11069-020-04203-5.

Renqvist, H., 1926. Ein Seebär in finnland. Zur frage nach der Entstehung der Seebären. Geogr. Ann. 8, 230–236.

Robertson, W.M., Kluver, D.B., Allen, J.T., Anderson, E.J., 2022. The hydrologic response to a meteotsunami in an isolated wetland: beaver Island in Lake Michigan, USA. J. Geophys. Res. Oceans 127. https://doi.org/10.1029/2022JC018611 e2022JC018611.

Schwegmann, S., Holfort, J., 2021. Regional distributed trends of sea ice volume in the Baltic Sea for the 30-year period 1982 to 2019. Meteorol. Z. 30, 33–43. https://doi.org/10.1127/metz/2020/0986.

Šepić, J., Vilibić, I., Monserrat, S., 2009. Teleconnections between the adriatic and the balearic meteotsunamis. Phys. Chem. Earth 34, 928–937. https://doi.org/10.1016/j.pce.2009.08.007.

Šepić, J., Vilibić, I., Strelec Mahović, N., 2012. Northern Adriatic meteorological tsunamis: observations, link to the atmosphere, and predictability. J. Geophys. Res. 117, C02002 https://doi.org/10.1029/2011JC007608.

Šepić, J., Rabinovich, A.B., 2014. Meteotsunami in the Great Lakes and on the atlantic coast of the United States generated by the "derecho" of June 29–30, 2012. Nat. Hazards 74, 75–107. https://doi.org/10.1007/s11069-014-1310-5.

Šepić, J., Vilibić, I., Lafon, A., Macheboeuf, L., Ivanović, Z., 2015. High-frequency sea level oscillations in the Mediterranean and their connection to synoptic patterns. Prog. Oceanogr. 137, 284–298. https://doi.org/10.1016/j.pocean.2015.07.005.

Šepić, J., Međugorac, I., Janeković, I., Dunić, N., Vilibić, I., 2016a. Multi-meteotsunami event in the Adriatic Sea generated by atmospheric disturbances of 25–26 June 2014. Pure Appl. Geophys. 173, 4117–4138. https://doi.org/10.1007/s00024-016-1249-4.

Šepić, J., Vilibić, I., Monserrat, S., 2016b. Quantifying the probability of meteotsunami occurrence from synoptic atmospheric patterns. Geophys. Res. Lett. 43, 10377–10384. https://doi.org/10.1002/2016GL070754.

Šepić, J., Orlić, M., Mihanović, H., 2022. Adriatic Meteotsunami Catalogue available at: https://projekti.pmfst.unist.hr/floods/meteotsunamis. (Accessed 26 September 2022).

Sergienko, O.V., 2010. Elastic response of floating glacier ice to impact of long-period ocean waves. J. Geophys. Res. Oceans 115, F04028. https://doi.org/10.1029/2010JF001721.

Shi, L.M., Olabarrieta, M., Nolan, D.S., Warner, J.C., 2020. Tropical cyclone rainbands can trigger meteotsunamis. Nat. Commun. 11, 678. https://doi.org/10.1038/s41467-020-14423-9.

Suursaar, U., Kullas, T., Otsmann, M., Saaremäe, I., Kuik, J., Merilain, M., 2006. Cyclone Gudrun in January 2005 and modelling its hydrodynamic consequences in the Estonian coastal waters. Boreal Environ. Res. 11, 143–159.

Taherkhani, M., Vitousek, S., Barnard, P.L., Frazer, N., Anderson, T.R., Fletcher, C.H., 2020. Sea-level rise exponentially increases coastal flood frequency. Sci. Rep. 10, 6466. https://doi.org/10.1038/s41598-020-62188-4.

Tanaka, K., 2010. Atmospheric pressure-wave bands around a cold front resulted in a meteotsunami in the East China Sea in February 2009. Nat. Hazards Earth Syst. Sci. 10, 2599–2610. https://doi.org/10.5194/nhess-10-2599-2010.

Thomson, R.E., Emery, W.J., 2014. Data Analysis Methods in Physical Oceanography. Elsevier, Amsterdam, p. 716. https://doi.org/10.1016/C2010-0-66362-0.

Ursell, F., 1952. Edge waves on a sloping beach. Proc. Roy. Soc. Lond. 214, 79–97. https://doi.org/10.1098/rspa.1952.0152.

Vennell, R., 2010. Resonance and trapping of topographic transient ocean waves generated by a moving atmospheric disturbance. J. Fluid Dynam. 650, 427–442. https://doi.org/10.1017/S0022112009993739.

Vilibić, I., 2008. Numerical simulations of the Proudman resonance. Continent. Shelf Res. 28, 574–581. https://doi.org/10.1016/j.csr.2007.11.005.

Vilibić, I., Šepić, J., 2009. Destructive meteotsunamis along the eastern Adriatic coast: overview. Phys. Chem. Earth 34, 904–917. https://doi.org/10.1016/j.pce.2009.08.004.

Vilibić, I., Šepić, J., 2017. Global mapping of nonseismic sea level oscillations at tsunami timescales. Sci. Rep. 7, 40818 https://doi.org/10.1038/srep40818.

Vilibić, I., Šepić, J., Ranguelov, B., Strelec Mahović, N., Tinti, S., 2010. Possible atmospheric origin of the 7 May 2007 western Black Sea shelf tsunami event. J. Geophys. Res. 115, C07006 https://doi.org/10.1029/2009JC005904.

Vilibić, I., Šepić, J., Dunić, N., Sevault, F., Monserrat, S., Jordà, G., 2018. Proxy-based assessment of strength and frequency of meteotsunamis in future climate. Geophys. Res. Lett. 45, 10501–10508. https://doi.org/10.1029/2018GL079566.

Vilibić, I., Denamiel, C., Zemunik, P., Monserrat, S., 2021. The mediterranean and Black Sea meteotsunamis: an overview. Nat. Hazards 106, 1223–1267. https://doi.org/10.1007/s11069-020-04306-z.

Williams, D.A., Schultz, D.M., Horsburgh, K.J., Hughes, C.W., 2021. An 8-yr meteotsunami climatology across Northwest Europe: 2010–17. J. Phys. Oceanogr. 51, 1145–1161. https://doi.org/10.1175/JPO-D-20-0175.1.

Witting, R., 1911. Tidvattnen i Östersjön och Finska viken. Fennia 29 (2), 1–84.

Wolski, T., Wiśniewski, B., Giza, A., Kowalewska-Kalkowska, H., Boman, H., Grabbi-Kaiv, S., Hammarklint, T., Holfort, J., Lydeikaite, Ž., 2014. Extreme sea levels at selected stations on the Baltic Sea coast. Oceanologia 56 (2), 259–290. https://doi.org/10.5697/oc.56-2.259.

Yankovsky, A.E., 2008. Large-scale edge waves generated by hurricane landfall. J. Geophys. Res. Oceans 114, C03014. https://doi.org/10.1029/2008JC005113.

Zemunik, P., Denamiel, C., Šepić, J., Vilibić, I., 2022a. High-frequency sea-level analysis: global distributions. Global Planet. Change 210, 103775. https://doi.org/10.1016/j.gloplacha.2022.103775.

Zemunik, P., Denamiel, C., Williams, J., Vilibić, I., 2022b. High-frequency sea-level extremes: global correlations to synoptic atmospheric patterns. Available at: SSRN [preprint]. https://doi.org/10.2139/ssrn.4075649.